



Institute of Theoretical Physics - Prof. Frédéric Mila

# Effect of Magnetic Field on Dynamics of Antiferromagnets

by  
Martin Mourigal

Master Thesis

Supervised by  
Dr. Mike Zhitomirsky  
DRFMC/SPSMS, CEA-Grenoble, France



JANUARY 2008

# Contents

<b>1</b>	<b>General outline and motivations</b>	<b>5</b>
<b>2</b>	<b>Beyond Linear Spin-Wave Theory</b>	<b>7</b>
2.1	First results on the Heisenberg Hamiltonian in an external magnetic field . . . .	7
2.1.1	Explicit form of the Hamiltonian . . . . .	7
2.1.2	The harmonic approximation . . . . .	9
2.2	Static properties beyond the Linear Spin-Wave Theory . . . . .	10
2.2.1	Contribution from quartic terms . . . . .	10
2.2.2	Contribution from renormalization of the canting angle . . . . .	10
2.2.3	Contribution from cubic part . . . . .	11
2.2.4	Magnetization curve . . . . .	12
2.3	Spectrum renormalization due to magnons interactions . . . . .	13
2.3.1	General properties of the excitation spectrum . . . . .	13
2.3.2	Magnons GREEN's function and perturbation theory . . . . .	13
2.3.3	Contribution from decay and source vertices . . . . .	14
2.3.4	Contribution from quartic terms and angle renormalization . . . . .	15
2.3.5	Renormalized spectrum . . . . .	16
<b>3</b>	<b>Kinematics of Magnons Decay</b>	<b>17</b>
3.1	Origin of decay . . . . .	17
3.2	Decay near the GOLDSTONE mode . . . . .	18
3.2.1	Curvature of the spectrum . . . . .	18
3.2.2	Computation of the threshold field . . . . .	18
3.3	Decay within the Brillouin zone . . . . .	19
3.3.1	Decay in magnons with equal momenta . . . . .	19
3.3.2	Decay surfaces . . . . .	20
3.4	Understanding decays with two-magnons density of states . . . . .	20
3.4.1	Van-Hove singularities in the two-magnons density of states . . . . .	21
3.4.2	Evolution of the density of states with magnetic field . . . . .	22
<b>4</b>	<b>Decay Dynamics</b>	<b>25</b>
4.1	A closer look at singularities . . . . .	25
4.1.1	Analytical properties of the Self-energy near divergences . . . . .	25
4.1.2	Finite lifetimes remove divergences . . . . .	27
4.2	Analytical expressions for magnons decay rates . . . . .	27
4.2.1	The Self-Consistent Born Approximation . . . . .	27
4.2.2	Magnons decay rates within the SCBA . . . . .	28
4.3	Numerical integration of self-consistent equations . . . . .	29

<b>5</b>	<b>Neutron scattering predictions</b>	<b>33</b>
5.1	Dynamical correlations functions . . . . .	33
5.2	Spin GREEN's function in the canted frame . . . . .	33
5.2.1	Longitudinal fluctuations . . . . .	34
5.2.2	Transverse fluctuations . . . . .	35
5.3	Measurable Spin Correlations . . . . .	37
5.3.1	Correlations functions within the SCBA . . . . .	37
5.3.2	Back to the laboratory . . . . .	38
<b>6</b>	<b>Conclusion</b>	<b>40</b>

# Abstract

Motivated by synthesis of new antiferromagnetic compounds with weak exchange coupling, a study of high magnetic field properties of the HEISENBERG model on a square-lattice is undertaken here. Ordered spins at zero temperature cant toward the field direction inducing coupling of transverse and longitudinal magnon modes. Resulting interactions renormalize the ground-state energy and the dispersion relation below a threshold field  $H^* = 0.76H_{sat}$ , where one-magnon excitations starts to become unstable and acquire finite lifetimes. Such decays originates from VAN-HOVE singularities in the two-magnons density of states lying below the one-particle energy. Decay rates are computed using a Self-Consistent BORN Approximation, revealing strong magnon damping in the middle of the BRILLOUIN's zone quarters whereas sound and precession modes remain well defined. Far from these modes, transverse part of the dynamical structure factor display important broadening of the excitations peaks that might be accesible to neutron scattering experiments.

# Acknowledgments

I first would like to express my gratitude to Mike ZHITOMIRSKY who accepted to supervise this diploma work. During these months, Mike had the patience, day after day, to explain and explain again, all these little and big things I would not have understood whithout his help. I hope that crossing the street to the ILL, I will not loose scientific contact with such an outstanding physicist.

This work was hosted at the "Service de Physique Statistique, Magnétisme and Supraconductivité" of CEA-Grenoble, and I am grateful to his director, Jean-Pascal Brison, for financial support I received. I also acknowledge other students and post-docs from the theory group, and especially Utpal, Sean, Raphael and Pierre-Eric, for sharing up and downs of laboratory life.

Finally, I would like to thank Frédéric Mila for being the university supervisor of this work and for his help while I was searching my way between theoretical or experimental physics. This diploma work and my future Ph.D project would not exist whithout his support and advices.

# Chapter 1

## General outline and motivations

Antiferromagnets belong to a class of materials where microscopic quantum effects are directly related to macroscopic properties. In such compounds, magnetic atoms interact through their spin and can display magnetic ordering. Due to increasing complexity with the number of interacting atoms, physics of antiferromagnets is very rich. Collective excitations in such systems can be theoretically understood with well-known models that describe coupling between spins, such as the HEISENBERG Hamiltonian. This model displays a large variety of ground-state and low-energy excitations depending on lattice geometry, dimensionality, spin value, or nature of the couplings. The case of spins one-half on a square lattice experienced a spectacular regain of interest after the discovery of high-temperature superconductors by BENDORZ & MÜLLER in 1986.

Compound	$Jk_b^{-1}(K)$	$H_c(T)$	$J'/J$
$\text{La}_2\text{CuO}_4$	$\cong 1500$	4500	$8.110^{-4}$
$\text{Cu}(\text{COO})_24\text{D}_2\text{O}$	71.8	220	$1.910^{-3}$
$(5\text{CAP})_2\text{CuBr}_4$	8.5	25.3	0.26
$(5\text{CAP})_2\text{CuCl}_4$	1.25	3.62	0.25
$(5\text{MAP})_2\text{CuCl}_4$	0.76	2.26	0.21

Table 1.1: Experimental magnetic properties [9] of different families of S=1/2 Heisenberg antiferromagnets on a square lattice.  $J$  is the nearest neighbour exchange constant,  $H_c = 8JS/g\mu_b$  the saturation field and  $J'$  the interlayer coupling. The  $J'/J$  ratio is obtained using extrapolation from quantum Monte-Carlo calculations and experimental data.

Some parent compounds of the superconducting cuprates, such as  $\text{La}_2\text{CuO}_4$ , are believed to be fair realizations of an HEISENBERG spin one-half square-lattice antiferromagnet with nearest neighbor coupling. This model has been intensively studied and is now well understood. Recently, progress in synthesis chemistry added new metal-organic compounds to the zoo of square-lattice spin one-half antiferromagnets [9]. Some experimental studies concentrated their efforts on specific compounds such as CFTD (Copper Formate TetraDeuterate : formulae  $\text{Cu}(\text{COO})_24\text{D}_2\text{O}$ ) due to significant reduction of the exchange constant  $J$  compared to  $\text{La}_2\text{CuO}_4$ . With reduction of coupling strength between spins, new experimental opportunities appeared, combined with breakthrough in neutron scattering techniques. The study of effects of magnetic field on long-range ordered HEISENBERG antiferromagnet is now achievable. This new possibilities originates

from lowering of saturation field (Table 1.1) to achievable magnetic field in neutron scattering facilities. Although common for quasi-one-dimensional antiferromagnets [3] [18] such studies are not well developed for bi- and tri- dimensional systems. Motivation to describe properties of square-lattice antiferromagnets under applied magnetic field is reinforced by the important role played by HEISENBERG Hamiltonian to describe spin one and spin five-half systems where single-ion anisotropy is weak.

The study of static properties such as magnetization and susceptibility has been carried out in [20] for a model with nearest neighbor coupling and a nice step ahead in understanding its low-energy excitations was performed by ZHITOMIRSKY and CHERNYCHEV in [5]. Based on this results, and with a restriction to the bidimensional case, the objective of this work is threefold. First, as magnetic field induces specific interactions between excitations, deviations from harmonicity are analysed with spin-wave theory (Chapter 2). Then, as excitations are believed to be unstable in high fields, their finite lifetime at zero-temperature is introduced (Chapter 3) and computed within the self-consistent Born approximation (Chapter 4). Finally, derived quantities are related to experiments in predicting possible neutron scattering dynamical structure factors (Chapter 5). Although inspired from previous works( [20] and [5]), this study introduce an explicit way to compute magnons decay rate which is of direct experimental relevance.

## Chapter 2

# Beyond Linear Spin-Wave Theory

### 2.1 First results on the Heisenberg Hamiltonian in an external magnetic field

The HEISENBERG Hamiltonian on a square-lattice under applied magnetic field and with nearest-neighbor interactions can be written:

$$\hat{\mathcal{H}} = J \sum_{\langle i,j \rangle} \mathbf{S}_i \cdot \mathbf{S}_j - H \sum_i S_i^{z_0} \quad (2.1)$$

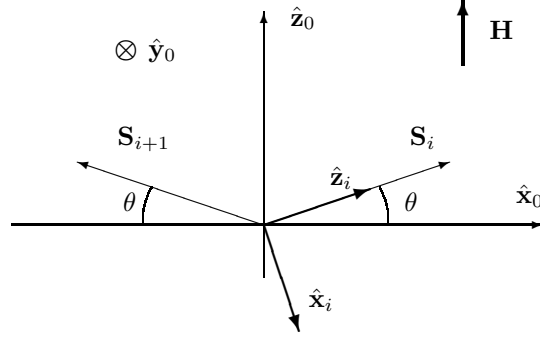
where  $J$  stands for the antiferromagnetic exchange coupling constant,  $\langle i,j \rangle$  restricts the sum to nearest-neighbor sites of the square lattice and  $H$  equals  $g\mu_b h$ , with  $h$  the intensity of a uniform external magnetic field directed toward axis  $z_0$ .

In the bidimensional isotropic case ( $H \rightarrow 0$  and  $D = 2$ ) and at zero temperature, it is proved [15] that Hamiltonian (2.1) displays long-range order (LRO) for all spin values  $S \geq 3/2$ . Furthermore, it is now commonly accepted that this property extends to lower spin values including 'quantum' ( $S = 1/2$ ) systems [13]. Nevertheless, for  $D \leq 2$  long-range order disappears at any finite temperature and for any spin value [14]. When isotropy is explicitly broken by external magnetic field and for  $D \geq 2$ , evolution from the ordered state is simple [20] as spins cant toward the field direction. Such a behavior *requires* an ordered ground state so that this study concerns  $D = 2$  models, with arbitrary spin, and at zero temperature. Tridimensional models also display long-range order at zero-temperature and consist of an extension of the results presented hereby.

#### 2.1.1 Explicit form of the Hamiltonian

In the zero-field phase of (2.1) interactions are not frustrated and spins arrange in the well-known NÉEL structure described by the ordering vector  $\mathbf{Q} = (\pi, \pi)$ . In the spin space, magnetic field is applied perpendicularly to vector  $\mathbf{Q}$  so that spins gradually rotate toward its direction. A spin operator in the laboratory frame  $(x_0, y_0, z_0)$  is related to its expression in the rotating frame  $(x_i, y_i, z_i)$  in the following way:

$$\begin{cases} \hat{S}_i^{x_0} = \hat{S}_i^x \sin \theta + \hat{S}_i^z \cos \theta e^{i\mathbf{Q} \cdot \mathbf{r}_i} \\ \hat{S}_i^{y_0} = \hat{S}_i^y \\ \hat{S}_i^{z_0} = -\hat{S}_i^x \cos \theta e^{i\mathbf{Q} \cdot \mathbf{r}_i} + \hat{S}_i^z \sin \theta \end{cases}$$



where  $\theta$  denotes the canting angle and  $\mathbf{r}_i$  the position of the site  $i$  on the lattice. On the contrary to several early studies [12] [17], the system is not divided into two sub-lattices and alternatively, the NÉEL ordering vector  $\mathbf{Q}$  is used to 'flip' spins directions ( $e^{i\mathbf{Q}\cdot\mathbf{r}_i} = \pm 1$  on the square lattice). In the rotating frame the Hamiltonian reads:

$$\begin{aligned} \hat{\mathcal{H}} = J \sum_{\langle i,j \rangle} & [-\cos 2\theta(S_i^x S_j^x + S_i^z S_j^z) + S_i^y S_j^y - \sin 2\theta e^{i\mathbf{Q}\cdot\mathbf{r}_i} (S_i^x S_j^z - S_i^z S_j^x)] \\ & + H \sum_i [S_i^x \cos \theta e^{i\mathbf{Q}\cdot\mathbf{r}_i} - S_i^z \sin \theta] \end{aligned} \quad (2.2)$$

Spin operators can be written *exactly* via bosonic operators using the HOLSTEIN-PRIMAKOFF transformation:

$$S_i^z = S - a_i^\dagger a_i, \quad S_i^+ = S_i^x + iS_i^y = \sqrt{2S - a_i^\dagger a_i} a_i, \quad S_i^- = S_i^x - iS_i^y = a_i^\dagger \sqrt{2S - a_i^\dagger a_i} \quad (2.3)$$

where  $a_i^\dagger$  creates a spin deviation on the site  $i$  and  $a_i$  annihilates it, provided  $a_i^\dagger a_i \leq 2S$ .

The so-called *Spin-Wave Theory* (SWT) consists in a series expansion of the square root involved in  $S_i^+$  and  $S_i^-$  while forgetting the constraints on operators so that  $a_i^\dagger a_i > 2S$  is allowed. At the 'linear'-order, this theory produced major achievements in the understanding of antiferromagnets [2] [12] and is believed to have good convergence toward 'exact' results estimated numerically using Monte-Carlo techniques [6]. Spin-wave theory actually corresponds to an  $1/S$  series expansion and is more likely to fail for small spins, where the second term of the series is not even small ( $1/S = 2$ ), than for large spins. This physically corresponds to enhanced quantum fluctuations for small spins, creating significative deviations from the 'classical' large-S results. In order to understand the effect of non-linearities on Hamiltonian (2.1), square root is expanded up to the second order as  $\sqrt{2S - a_i^\dagger a_i} = \sqrt{2S} \left(1 - \frac{a_i^\dagger a_i}{4S}\right)$  and the Hamiltonian reads:

$$\hat{\mathcal{H}} = \hat{\mathcal{H}}_0 + \hat{\mathcal{H}}_1 + \hat{\mathcal{H}}_2 + \hat{\mathcal{H}}_3 + \hat{\mathcal{H}}_4 + \dots \quad (2.4)$$

where  $\hat{\mathcal{H}}_n = \mathcal{O}(S^{2-n/2})$  contains all terms with  $n$   $a$  or  $a^\dagger$  operators. As the Hamiltonian (2.2) contains mixed  $x - z$  terms, odd powers of the expansion (2.4) do not vanish. This originates from the *non-collinear* order induced by the field and can also appear on triangular lattices at zero field, where spins form the so called '120°-structure' [1]. Combining (2.2) and (2.3), one can derive the following expressions contributing to the 'harmonic' part of the Hamiltonian:

$$\epsilon_0 = \hat{\mathcal{H}}_0/N = -2JS^2 \cos 2\theta - HS \sin \theta \quad (2.5)$$

$$\hat{\mathcal{H}}_1 = \sqrt{\frac{S}{2}} \cos \theta (H - 8JS \sin \theta) \sum_i e^{i\mathbf{Q}\cdot\mathbf{r}_i} (a_i + a_i^\dagger) \quad (2.6)$$



$$\hat{\mathcal{H}}_2 = H \sin \theta \sum_i a_i^\dagger a_i + \frac{J}{2S} \sum_{i,j(i)} \left[ \cos 2\theta (a_i^\dagger a_i + a_j^\dagger a_j) + \sin^2 \theta (a_i^\dagger a_j + a_j^\dagger a_i) - \cos 2\theta (a_i^\dagger a_i^\dagger + a_j^\dagger a_j^\dagger) \right] \quad (2.7)$$

where  $j(i)$  stands for the index of the *four* nearest-neighbors of lattice site  $i$ , and  $\epsilon_0$  is the classical energy *per spin*. Higher order terms introduce *interactions* between spins deviations in going beyond the harmonic approximation:

$$\hat{\mathcal{H}}_3 = J \sin 2\theta \sqrt{\frac{S}{2}} \sum_{i,j(i)} (a_i^\dagger + a_i) a_j^\dagger a_j + \cos \theta \sqrt{\frac{S}{2}} \left( 2J \sin \theta - \frac{H}{4S} \right) \sum_i e^{i\mathbf{Q}\cdot\mathbf{r}_i} (a_i^\dagger n_i + n_i a_i) \quad (2.8)$$

$$\hat{\mathcal{H}}_4 = \frac{J}{2} \sum_{i,j(i)} \left[ -n_i n_j \cos 2\theta + \frac{1}{4} \cos^2 \theta \{ (n_i + n_j) a_i a_j + \text{h.c.} \} - \frac{1}{4} \sin^2 \theta \{ a_i^\dagger (n_i + n_j) a_j + \text{h.c.} \} \right] \quad (2.9)$$

where h.c. stands for Hermitian conjugate and  $n_i = a_i^\dagger a_i$ .

### 2.1.2 The harmonic approximation

The linear or 'harmonic' approximation (LSWT) neglects all terms of order higher than  $\mathcal{O}(1/S^0) = \mathcal{O}(1)$ . From a classical point of view the energy per spin:

$$E_0(\theta) = 4JS^2 \sin^2 \theta - HS \sin \theta - 2JS^2 \quad \text{is minimum for} \quad \sin \theta_0 = \frac{H}{8JS} \quad (2.10)$$

which implies that spins smoothly cant toward the field direction and are all aligned for  $H_{sat} = 8JS$ . In the saturated phase, the ground state aspect is similar to the ferromagnetic case. For a classically selected canting angle, contribution  $\hat{\mathcal{H}}_1(\theta_0)$  vanishes. Renormalized contributions to the canting angle due to interactions are of higher orders in  $1/S$  and are not included in the LSWT. Using FOURIER transformed expressions for bosonic operators defined as  $a_{\mathbf{k}} = 1/N \sum_i a_i \exp(i\mathbf{k} \cdot \mathbf{r}_i)$ , the quadratic Hamiltonian reads:

$$\hat{\mathcal{H}}_2 = \sum_{\mathbf{k}} \left[ A_{\mathbf{k}} a_{\mathbf{k}}^\dagger a_{\mathbf{k}} - \frac{B_{\mathbf{k}}}{2} (a_{\mathbf{k}} a_{-\mathbf{k}} + a_{\mathbf{k}}^\dagger a_{-\mathbf{k}}^\dagger) \right] \quad (2.11)$$

where  $A_{\mathbf{k}} \equiv 4JS(1 + \sin^2 \theta_0 \gamma_{\mathbf{k}})$ ,  $B_{\mathbf{k}} \equiv 4JS \cos^2 \theta_0 \gamma_{\mathbf{k}}$ , and  $\gamma_{\mathbf{k}}$  is the sum of the *lattice harmonics*,  $\gamma_{\mathbf{k}} \equiv 1/4 \sum_{j(i)} \exp(i\mathbf{k} \cdot \mathbf{r}_j)$ . For bidimensional square-lattice with nearest-neighbor exchange,  $\gamma_{\mathbf{k}} = \frac{1}{2}(\cos k_x + \cos k_y)$ . Hamiltonian (2.11) is said to be harmonic as one can diagonalize it using the BOGOLIUBOV canonical transformation:

$$\begin{pmatrix} a_{\mathbf{k}} \\ a_{\mathbf{k}}^\dagger \end{pmatrix} = \begin{pmatrix} u_{\mathbf{k}} & v_{\mathbf{k}} \\ u_{\mathbf{k}}^* & v_{\mathbf{k}}^* \end{pmatrix} \begin{pmatrix} b_{\mathbf{k}} \\ b_{-\mathbf{k}}^\dagger \end{pmatrix} \quad (2.12)$$

Due to the properties of FOURIER transform,  $u_{\mathbf{k}}^* = u_{-\mathbf{k}}$  and  $v_{\mathbf{k}}^* = v_{-\mathbf{k}}$ . Moreover  $b_{\mathbf{k}}^\dagger$  and  $b_{\mathbf{k}}$  follows bosonic commutations rules provided matrix (2.12) is unitary with real coefficients. As a result  $u_{\mathbf{k}} = u_{-\mathbf{k}}$ ,  $v_{\mathbf{k}} = v_{-\mathbf{k}}$  and  $u_{\mathbf{k}}^2 - v_{\mathbf{k}}^2 = 1$  so that the harmonic hamiltonian reads:

$$\hat{\mathcal{H}}_2 = \sum_{\mathbf{k}} \epsilon_{\mathbf{k}} b_{\mathbf{k}}^\dagger b_{\mathbf{k}} + \frac{1}{2} \sum_{\mathbf{k}} (\epsilon_{\mathbf{k}} - A_{\mathbf{k}}) \quad \text{with} \quad \epsilon_{\mathbf{k}} = 4JS \sqrt{(1 + \gamma_{\mathbf{k}})(1 - \cos 2\theta \gamma_{\mathbf{k}})}. \quad (2.13)$$

whereas the coefficient of the BOGOLIUBOV transformation can be expressed as:

$$u_{\mathbf{k}} = \sqrt{\frac{|A_{\mathbf{k}}|}{2\epsilon_{\mathbf{k}}} + 1} \quad \text{and} \quad v_{\mathbf{k}} = \text{sign}(\gamma_{\mathbf{k}}) \sqrt{u_{\mathbf{k}}^2 - 1} \quad (2.14)$$

First term in the Hamiltonian (2.13) is diagonal in terms of BOGOLIUBOV operators so that its ground-state  $|0\rangle$  is defined as  $b_{\mathbf{k}}|0\rangle = 0$ . Quasiparticles created on the ground state by  $b_{\mathbf{k}}^\dagger|0\rangle = |\mathbf{k}\rangle$  are the so-called *magnons*. Second term in (2.13) corresponds to purely quantum zero-point energy. The ground state energy in the LSWT is therefore  $E_{g.s}^{(2)} = E_o + \langle \hat{\mathcal{H}}_2 \rangle$

## 2.2 Static properties beyond the Linear Spin-Wave Theory

### 2.2.1 Contribution from quartic terms

In the zeroth order in perturbation theory,  $\hat{\mathcal{H}}_4$  has a non zero expectation value on the ground state  $\langle 0|\hat{\mathcal{H}}_4|0\rangle$ . Average value can be taken directly on equation (2.9) using WICK's theorem to pair bosonic  $a$ -operators. Using the HARTREE-FOCK averages defined as:

$$n = \langle a_i^\dagger a_i \rangle, m = \langle a_i^\dagger a_j \rangle, \delta = \langle a_i^2 \rangle \text{ and } \Delta = \langle a_i a_j \rangle \quad (2.15)$$

one can easily compute the different averages,  $\langle n_i n_j \rangle = n^2 + m^2 + \Delta^2$ ,  $\langle (n_i + n_j) a_i a_j \rangle = 8n\Delta + 4m\delta$  and  $\langle a_i^\dagger (n_i + n_j) a_j^\dagger \rangle = 8nm + 4\delta\Delta$  that yields :

$$\delta E_{g.s}^{(4)} = \langle 0|\hat{\mathcal{H}}_4|0\rangle = 2J [\cos^2 \theta (2n\Delta + \delta m) - \cos 2\theta (n^2 + \Delta^2 + m^2) - \sin^2 \theta (2nm + \delta\Delta)]$$

The HARTREE-FOCK averages of equation (2.15) can be numerically evaluated after BOGOLIUBOV transformation. Integration in the reciprocal space is done using SIMPSONS integration technique with enhanced number of points around the  $\mathbf{k} = \mathbf{Q}$  point where integrand as logarithmic singularity : some results are presented on Table (2.1).

Field	0	0.50 $H_{sat}$	0.75 $H_{sat}$
$n = \sum_{\mathbf{k}} v_{\mathbf{k}}^2$	0.196602	0.0936446	0.0537367
$m = \sum_{\mathbf{k}} \gamma_{\mathbf{k}} v_{\mathbf{k}}^2$	0.0000000	-0.0571777	-0.0428606
$\delta = \sum_{\mathbf{k}} u_{\mathbf{k}} v_{\mathbf{k}}$	0.0000000	-0.0834939	-0.0784327
$\Delta = \sum_{\mathbf{k}} \gamma_{\mathbf{k}} u_{\mathbf{k}} v_{\mathbf{k}}$	0.275576	0.162442	0.106100

Table 2.1: HARTREE-FOCK averages with two-dimensional integrals computed on a  $10^5 \times 10^5$  points bidimensional BRILLOUIN ZONE

### 2.2.2 Contribution from renormalization of the canting angle

WICK's theorem can also be fruitfully applied to  $\langle 0|\hat{\mathcal{H}}_3|0\rangle$ . The second part of equation (2.8) vanishes at the equilibrium value of the canting angle, so that after decoupling of the form  $\langle (a_i^\dagger + a_i) a_j^\dagger a_j \rangle = n(a_i^\dagger + a_i) + (\delta + m)(a_j^\dagger + a_j)$  and FOURIER transform:

$$\langle \hat{\mathcal{H}}_3 \rangle = \hat{\mathcal{H}}_3^{(1)} = 4J \sin 2\theta \sqrt{\frac{S}{2}} (n - m - \Delta) (a_{\mathbf{Q}}^\dagger + a_{\mathbf{Q}})$$

Such linear Hamiltonian contributes to the ground-state energy as it *renormalizes* the canting angle. Linear terms in  $a$ -operators must disappear in the expression of the ground state energy, so that coefficients of such operators in the 'full' linear term  $\hat{\mathcal{H}}_1 + \hat{\mathcal{H}}_3^{(1)}$  must vanish. Such cancellation yields the expression for the renormalized angle :

$$\sin \theta = \sin \theta_0 \left[ 1 + \frac{n - m - \Delta}{S} \right]$$

This slight change in the angle contributes to the ground-state energy in two ways. First, it shifts the classical energy of a value:

$$\delta E_{g.s}^{(0)} = 4JS^2(\sin \theta_0 - \sin \theta)^2 = \frac{H^2}{16JS^2}(n - m - \Delta)^2 \equiv \mathcal{O}\left(\frac{1}{S^2}\right)$$

so that it was reasonable to neglect such angle renormalization in the LSWT. Then, it shifts the  $A_{\mathbf{k}}$  and  $B_{\mathbf{k}}$  coefficients in  $\hat{\mathcal{H}}_2$  by quantities  $\delta A_{\mathbf{k}} = -\frac{H^2}{8JS^2}(1 - \gamma_{\mathbf{k}})(n - m - \Delta)$  and  $\delta B_{\mathbf{k}} = -\frac{H^2}{8JS^2}\gamma_{\mathbf{k}}(n - m - \Delta)$  resulting in the following shift of the ground-state energy from the quadratic part:

$$\delta E_{g.s}^{(2)} = \langle \delta \hat{\mathcal{H}}_2 \rangle = -\frac{H^2}{8JS^2}(n - m - \Delta)^2$$

### 2.2.3 Contribution from cubic part

Contributions from cubic term at the first order in perturbation theory have already been included through consequences of angle renormalization on the ground state energy. However, cubic term also contributes to the ground-state energy at the second order in perturbation theory. In order to apply RAYLEIGH-SCHRODINGER theory it is first required to apply BOGOLIUBOV transformation to  $\hat{\mathcal{H}}_3$ . Starting from the following FOURIER transformed equation:

$$\hat{\mathcal{H}}_3 = -\frac{H \cos \theta}{\sqrt{2SN}} \sum_{\mathbf{k}, \mathbf{q}} \gamma_{\mathbf{k}} \left( a_{\mathbf{k}+\mathbf{q}-\mathbf{Q}}^\dagger a_{\mathbf{q}}^\dagger a_{\mathbf{k}} + a_{\mathbf{k}}^\dagger a_{\mathbf{q}}^\dagger a_{\mathbf{k}+\mathbf{q}-\mathbf{Q}} \right) \quad (2.16)$$

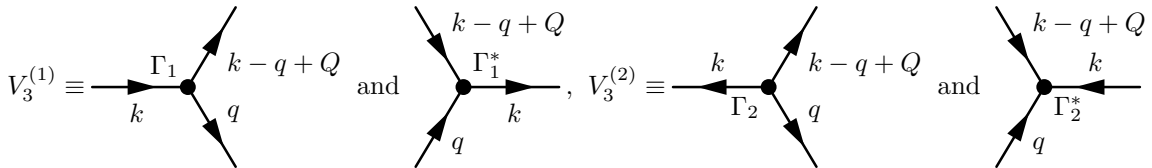
one can derive the following cubic terms constituting the lowest order interaction between magnons, explicitly written in terms of creation and annihilation operators [5]:

$$\begin{aligned} \hat{V}_3^{(1)} &= \frac{1}{2!} \sum_{\mathbf{k}, \mathbf{q}} \left\{ \Gamma_1(\mathbf{k}, \mathbf{q}) \left[ b_{\mathbf{k}-\mathbf{q}+\mathbf{Q}}^\dagger b_{\mathbf{q}}^\dagger b_{\mathbf{k}} \right] + \Gamma_1^*(\mathbf{k}, \mathbf{q}) \left[ b_{\mathbf{k}}^\dagger b_{\mathbf{q}} b_{\mathbf{k}-\mathbf{q}+\mathbf{Q}} \right] \right\} \\ \hat{V}_3^{(2)} &= \frac{1}{3!} \sum_{\mathbf{k}, \mathbf{q}} \left\{ \Gamma_2(\mathbf{k}, \mathbf{q}) \left[ b_{\mathbf{k}}^\dagger b_{\mathbf{q}}^\dagger b_{\mathbf{k}-\mathbf{q}+\mathbf{Q}} \right] + \Gamma_2^*(\mathbf{k}, \mathbf{q}) \left[ b_{\mathbf{k}} b_{\mathbf{q}} b_{\mathbf{k}-\mathbf{q}+\mathbf{Q}} \right] \right\} \end{aligned} \quad (2.17)$$

where the vertices  $\Gamma_1(\mathbf{k}, \mathbf{q})$  and  $\Gamma_2(\mathbf{k}, \mathbf{q})$  have the following expressions:

$$\begin{aligned} \Gamma_1(\mathbf{k}, \mathbf{q}) &= -\frac{H \cos \theta}{\sqrt{2SN}} \left[ \gamma_{\mathbf{k}}(u_{\mathbf{k}} + v_{\mathbf{k}})(u_{\mathbf{q}}v_{\mathbf{k}-\mathbf{q}+\mathbf{Q}} + v_{\mathbf{q}}u_{\mathbf{k}-\mathbf{q}+\mathbf{Q}}) \right. \\ &\quad \left. + \gamma_{\mathbf{q}}(u_{\mathbf{q}} + v_{\mathbf{q}})(u_{\mathbf{k}}u_{\mathbf{k}-\mathbf{q}+\mathbf{Q}} + v_{\mathbf{k}}v_{\mathbf{k}-\mathbf{q}+\mathbf{Q}}) + \gamma_{\mathbf{k}-\mathbf{q}+\mathbf{Q}}(u_{\mathbf{k}-\mathbf{q}+\mathbf{Q}} + v_{\mathbf{k}-\mathbf{q}+\mathbf{Q}})(u_{\mathbf{k}}u_{\mathbf{q}} + v_{\mathbf{k}}v_{\mathbf{q}}) \right] \\ \Gamma_2(\mathbf{k}, \mathbf{q}) &= -\frac{H \cos \theta}{\sqrt{2SN}} \left[ \gamma_{\mathbf{k}}(u_{\mathbf{k}} + v_{\mathbf{k}})(u_{\mathbf{q}}v_{\mathbf{k}-\mathbf{q}+\mathbf{Q}} + v_{\mathbf{q}}u_{\mathbf{k}-\mathbf{q}+\mathbf{Q}}) \right. \\ &\quad \left. + \gamma_{\mathbf{q}}(u_{\mathbf{q}} + v_{\mathbf{q}})(u_{\mathbf{k}}v_{\mathbf{k}-\mathbf{q}+\mathbf{Q}} + v_{\mathbf{k}}u_{\mathbf{k}-\mathbf{q}+\mathbf{Q}}) + \gamma_{\mathbf{k}-\mathbf{q}+\mathbf{Q}}(u_{\mathbf{k}-\mathbf{q}+\mathbf{Q}} + v_{\mathbf{k}-\mathbf{q}+\mathbf{Q}})(u_{\mathbf{k}}v_{\mathbf{q}} + v_{\mathbf{k}}u_{\mathbf{q}}) \right] \end{aligned}$$

Such vertices correspond to interaction between one-magnon  $|\mathbf{k}\rangle$  and two-magnons  $|\mathbf{q}, \mathbf{k} - \mathbf{q} + \mathbf{Q}\rangle$  states via the following events:



so that  $\hat{V}_3^{(1)}$  introduce *decay* processes and  $\hat{V}_3^{(2)}$  *source* ones. From diagrams, one can realize that vertex  $\Gamma_1$  is symmetric with respect to exchange of two incoming (or outgoing) momenta. Writing  $\Gamma_1$  in a symmetric form with respect to such permutation requires to divide the actual interaction by the number of equivalent diagrams. They are 3 choices of incoming momentum

that yields non-equivalent diagrams on a total number of  $3!$  diagrams. The  $\hat{V}_3^{(1)}$  is therefore normalized by a factor  $3 \cdot \frac{1}{3!} = \frac{1}{2!}$ . On the other hand,  $\Gamma_2$  is fully symmetric with respect to exchange of momenta so that  $\hat{V}_3^{(2)}$  is normalized by a factor  $\frac{1}{3!}$ .

It is now easy to apply perturbation theory up to the second order and obtain contribution to the ground-state energy:

$$\delta E_{g.s}^{(3)} = \sum_{\mathbf{p}_1, \mathbf{p}_2, \mathbf{p}_3} \frac{|\langle \mathbf{p}_1, \mathbf{p}_2, \mathbf{p}_3 | \hat{V}_3^{(1)} + \hat{V}_3^{(2)} | 0 \rangle|^2}{E_{g.s}^{(0)} - (\epsilon_{\mathbf{p}_1} + \epsilon_{\mathbf{p}_2} + \epsilon_{\mathbf{p}_3})} = -3! \frac{1}{(3!)^2} \sum_{\mathbf{k}, \mathbf{q}} \frac{|\Gamma_2(\mathbf{k}, \mathbf{q})|^2}{\epsilon_{\mathbf{k}} + \epsilon_{\mathbf{q}} + \epsilon_{\mathbf{k}-\mathbf{q}+\mathbf{Q}}} \quad (2.18)$$

where  $\hat{V}_3^{(1)}$  does not contribute to the ground-state energy while the factor  $3!$  corresponds to the number of possible permutations giving  $\langle \mathbf{p}_1, \mathbf{p}_2, \mathbf{p}_3 | \mathbf{k}, \mathbf{q}, \mathbf{k} - \mathbf{q} + \mathbf{Q} \rangle \neq 0$ . Contribution (2.18) is of order  $1/S^2$  in the spin wave expansion so that at this order, the ground-state energy changes and becomes:

$$E_{g.s} = \delta E_o + \langle \hat{\mathcal{H}}_2 \rangle + \delta E_{g.s}^{(0)} + \delta E_{g.s}^{(2)} + \delta E_{g.s}^{(3)} \quad (2.19)$$

## 2.2.4 Magnetization curve

In the LSWT, the magnetization is obtained by differentiating the ground-state energy with respect to magnetic field and its expression is simple:

$$\frac{M}{S} = \frac{H}{H_{sat}} \left[ 1 - \frac{1}{2S} \sum_{\mathbf{k}} \gamma_{\mathbf{k}} \sqrt{\frac{1 + \gamma_{\mathbf{k}}}{1 - \gamma_{\mathbf{k}} \cos 2\theta}} \right] \quad (2.20)$$

Corrections to the ground-state energy contributes to renormalize the magnetization curve but the overall correction is small. The static properties of the HEISENBERG Hamiltonian can therefore be understood qualitatively within the harmonic regime. The magnetization curve has logarithmic singularity near the saturation field and the g characteristic shape [20] presented on Figure 2.1.

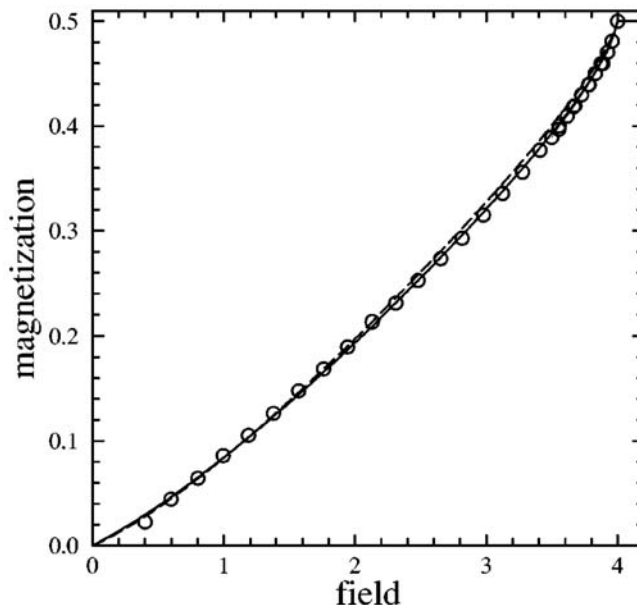


Figure 2.1: Magnetization curve for  $S = 1/2$ . Field is in unit of  $J$ . Dashed and solid lines are results at the first- and second-order in the spin-wave expansion

## 2.3 Spectrum renormalization due to magnons interactions

### 2.3.1 General properties of the excitation spectrum

In the Linear Spin-Wave Theory, low-energy excitations are the so-called *magnons* and can be considered as *free, bosonic-type*, quasiparticles. On the contrary to other bosonic systems such as superfluid Helium-4 or diluted Alkali atoms where coupling with BOSE-EINSTEIN condensate fixes the number of particles, magnons can be treated in a statistical ensemble where their number is not conserved. In zero-field, it is assumed that the system displays long-range order. This requires the continuous SU(2) symmetry of the Hamiltonian to be *spontaneously* broken. As a consequence from a well-know theorem known as the GOLDSTONE theorem, it is possible to create low-energy excitations so that the spectrum be *gapless*. This property remains true for non-zero magnetic field. For  $H = 0$ , zero-energy modes lies in  $\mathbf{k} = 0$  and  $\mathbf{k} = \mathbf{Q}$  whereas in the canted phase, only the  $\mathbf{k} = \mathbf{Q}$  mode remains gapless. This mode is rather called GOLDSTONE mode or *sound-mode* by analogy with phonon spectra in solids. The dispersion relation in the LSWT is plotted on Figure (2.2) for different magnetic field using its analytical expression:

$$\epsilon_{\mathbf{k}} = 4JS\omega_{\mathbf{k}} \quad \text{with} \quad \omega_{\mathbf{k}} = \sqrt{(1 + \gamma_{\mathbf{k}})(1 - \cos 2\theta\gamma_{\mathbf{k}})} \quad (2.21)$$

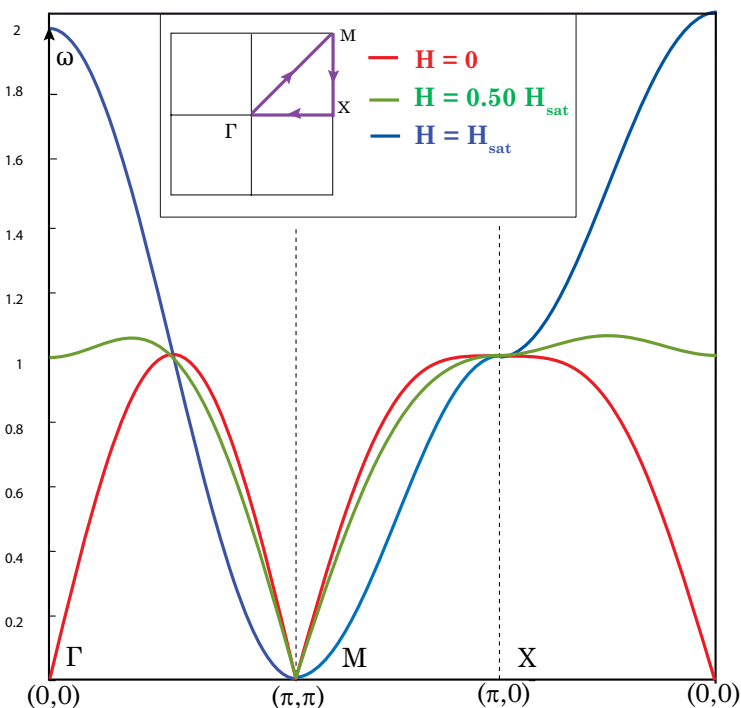


Figure 2.2: BRILLOUIN zone plot of dimensionless dispersion  $\omega_{\mathbf{k}}$  in the LSWT and for different magnetic fields.

### 2.3.2 Magnons Green's function and perturbation theory

In order to understand effects of interactions on the dispersion relation it is fruitful to use the formalism of Quantum Field Theory. As a first step, it is necessary to introduce magnons GREEN's functions. Precise derivations for bosons in presence of a Bose condensate, in the context of superfluid Helium 4, can be found in various textbooks [7] [8]. As discussed before,

the case of magnons is much simpler as their number is not conserved. Starting from the harmonic part of the Hamiltonian  $\hat{\mathcal{H}}_2 = \sum_{\mathbf{k}} \epsilon_{\mathbf{k}} b_{\mathbf{k}}^{\dagger} b_{\mathbf{k}}$  and using the general definition of GREEN's function for a system with translational invariance,

$$\mathcal{G}^{(0)}(\mathbf{x}, t) = -i \langle 0 | T b(\mathbf{x}, t) b^{\dagger}(\mathbf{0}, 0) | 0 \rangle$$

one can derive the following expression for *unperturbed* advanced and retarded magnon GREEN's functions:

$$\mathcal{G}^{(0)}(\mathbf{x}, t > 0) = -\frac{i}{N} \sum_{\mathbf{k}} e^{i(\mathbf{k} \cdot \mathbf{x} - \epsilon_{\mathbf{k}} t)} \langle 0 | b_{\mathbf{k}} b_{\mathbf{k}}^{\dagger} | 0 \rangle \neq 0 \quad (2.22)$$

$$\mathcal{G}^{(0)}(\mathbf{x}, t < 0) = -\frac{i}{N} \sum_{\mathbf{k}} e^{i(\mathbf{k} \cdot \mathbf{x} - \epsilon_{\mathbf{k}} t)} \langle 0 | b_{\mathbf{k}}^{\dagger} b_{\mathbf{k}} | 0 \rangle = 0 \quad (2.23)$$

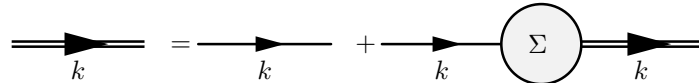
In (2.22) and (2.23),  $|0\rangle$  stands for the unperturbed ground state of the system. As a result of bosonic operators commutation rules, the retarded Green's function obviously vanishes. Furthermore, it is possible by coordinate and time Fourier transform to derive the following expression for the unperturbed GREEN's function :

$$\mathcal{G}^{(0)}(\mathbf{k}, \epsilon) = i \lim_{\delta \rightarrow 0^+} \int_0^{\infty} dt e^{it(\epsilon - \epsilon_{\mathbf{k}} + i\delta)} = \frac{1}{\epsilon - \epsilon_{\mathbf{k}} + i0^+} \quad (2.24)$$

In the expression of the *full* GREEN's function the projection on ground-state  $|0\rangle$  is substituted with projection on the interacting ground state. The strength of the technique is to go back to an average value on the unperturbed ground-state using perturbative expansion in powers of the interaction potential [8]:

$$\mathcal{G}(\mathbf{k}, t) = -i \langle T b_{\mathbf{k}}(t) b_{\mathbf{k}}^{\dagger} \rangle = -i \sum_{m=0}^{\infty} \frac{(-i)^m}{m!} \int dt_1 \dots dt_m \langle 0 | T \hat{V}(t_1) \dots \hat{V}(t_m) b_{\mathbf{k}}(t) b_{\mathbf{k}}^{\dagger} | 0 \rangle_{con} \quad (2.25)$$

where the sum is performed on all the *connected* diagrams that might appear in the expansion. In this context, it is possible to define the *self-energy* in the following schematical way using DYSON's equation [8]:

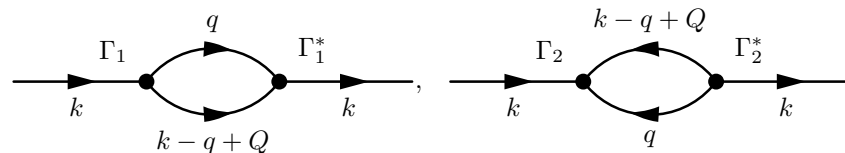


$$\text{Double line } k = \text{Single line } k + \text{Single line } k \text{ --- } (\Sigma) \text{ --- Double line } k \quad (2.26)$$

where thin lines stands for unperturbed magnon GREEN's function and double lines for full ones. Diagram (2.26) is a fancy way to write the basic equation  $\mathcal{G}(\mathbf{k}, \epsilon)^{-1} = \mathcal{G}^o(\mathbf{k}, \epsilon)^{-1} - \Sigma(\mathbf{k}, \epsilon)$ . The *renormalized* spectrum  $\tilde{\epsilon}$  corresponds to the poles of the perturbed GREEN's function so that it is solution of  $\tilde{\epsilon} = \epsilon_{\mathbf{k}} + \Sigma(\mathbf{k}, \tilde{\epsilon})$ , where  $\epsilon_{\mathbf{k}}$  corresponds to the harmonic dispersion. It is legitimate to neglect *anomalous* GREEN's function involving two creation or annihilation operators [6] so that the expansion only contains normal functions.

### 2.3.3 Contribution from decay and source vertices

The lowest order correction to the spectrum corresponds to interaction via cubic vertices  $V_3^{(1)}$  and  $V_3^{(2)}$ . This non-zero corrections corresponds to the following diagrams:



$$\text{Diagram 1: } \text{Line } k \text{ --- } \Gamma_1 \text{ --- Loop } (q, k-q+Q) \text{ --- } \Gamma_1^* \text{ --- Line } k \text{, Diagram 2: } \text{Line } k \text{ --- } \Gamma_2 \text{ --- Loop } (k-q+Q, q) \text{ --- } \Gamma_2^* \text{ --- Line } k \quad (2.27)$$

The self-energies associated with such diagrams are denoted  $\Sigma_{11}^{(1)}$  for the decay process and  $\Sigma_{11}^{(2)}$  for the source process. The "11" index means that this corrections come from normal GREEN's functions. Using FEYNMAN rules in momentum space [8] yields:

$$\begin{aligned}\Sigma_{11}^{(1)}(\mathbf{k}, \epsilon) &= 2i \frac{1}{(2!)^2} \sum_{\mathbf{q}} \int \frac{d\epsilon'}{2\pi} |\Gamma_1(\mathbf{k}, \mathbf{q})|^2 \mathcal{G}^o(\mathbf{k}, \epsilon') \mathcal{G}^o(\mathbf{k} - \mathbf{q} + \mathbf{Q}, \epsilon - \epsilon') \\ &= \frac{1}{2} \sum_{\mathbf{q}} \frac{|\Gamma_1(\mathbf{k}, \mathbf{q})|^2}{\epsilon - \epsilon_{\mathbf{q}} - \epsilon_{\mathbf{k}-\mathbf{q}+\mathbf{Q}} + i0} = 4J \sin^2 \theta \cos^2 \theta \sum_{\mathbf{q}} \frac{|\tilde{\Gamma}_1(\mathbf{k}, \mathbf{q})|^2}{\omega - \omega_{\mathbf{q}} - \omega_{\mathbf{k}-\mathbf{q}+\mathbf{Q}} + i0}\end{aligned}\quad (2.28)$$

$$\begin{aligned}\Sigma_{11}^{(2)}(\mathbf{k}, \epsilon) &= 18i \frac{1}{(3!)^2} \sum_{\mathbf{q}} \int \frac{d\epsilon'}{2\pi} |\Gamma_2(\mathbf{k}, \mathbf{q})|^2 \mathcal{G}^o(\mathbf{k}, \epsilon') \mathcal{G}^o(\mathbf{k} - \mathbf{q} + \mathbf{Q}, -\epsilon - \epsilon') \\ &= -\frac{1}{2} \sum_{\mathbf{q}} \frac{|\Gamma_2(\mathbf{k}, \mathbf{q})|^2}{\epsilon + \epsilon_{\mathbf{q}} + \epsilon_{\mathbf{k}-\mathbf{q}+\mathbf{Q}} - i0} = -4J \sin^2 \theta \cos^2 \theta \sum_{\mathbf{q}} \frac{|\tilde{\Gamma}_2(\mathbf{k}, \mathbf{q})|^2}{\omega + \omega_{\mathbf{q}} + \omega_{\mathbf{k}-\mathbf{q}+\mathbf{Q}} - i0}\end{aligned}\quad (2.29)$$

where dimensionless expressions for dispersion and vertices are  $\epsilon_{\mathbf{k}} = 4JS\omega_{\mathbf{k}}$  and  $\Gamma_{1,(2)} = -H \cos \theta / \sqrt{2S} \tilde{\Gamma}_{1,(2)}$  so that this corrections are of order  $\mathcal{O}(1/S^2)$ .

### 2.3.4 Contribution from quartic terms and angle renormalization

Contribution from quartic term  $\hat{\mathcal{H}}_4$  to the self-energy, computed at the first order in perturbation theory contains 6 bosonic operators. In order to compute its value on the unperturbed ground-state, WICK's theorem should be used. Once two operators from  $\hat{\mathcal{H}}_4$  are paired with the original field operators, there is no freedom for the remaining pairing. Choosing this pairing before BOGOLIUBOV transformation simplifies the whole computation. Applied to (2.9) this trick gives:

$$\begin{aligned}\delta \hat{\mathcal{H}}_4 &= \frac{J}{2} \sum_{i,j(i)} \left[ a_i^\dagger a_i a_j^\dagger a_j (n \cos 2\theta + \Delta \cos^2 \theta - m \sin^2 \theta) + (a_i^\dagger a_j a_j^\dagger a_i) \left( \frac{1}{2} \delta \cos^2 \theta - n \sin^2 \theta - m \cos 2\theta \right) \right. \\ &\quad \left. + (a_i a_j + a_i^\dagger a_i^\dagger) \left( n \cos^2 \theta - \Delta \cos 2\theta - \frac{1}{2} \delta \sin^2 \theta \right) + \frac{1}{4} (a_i^2 a_j^2 + a_i^{2\dagger} a_i^{2\dagger}) (m \cos^2 \theta - \Delta \sin^2 \theta) \right]\end{aligned}$$

Next step is to apply BOGOLIUBOV transformation while forgetting "anomalous" terms that do not contribute at the first order in perturbation theory. Finally, the quartic part of the Hamiltonian yields the following correction to the spectrum:

$$\begin{aligned}\delta \epsilon_{\mathbf{k}}^{(1)} &= \frac{4J}{\omega_{\mathbf{k}}} \left[ -n \cos 2\theta + \Delta \cos^2 \theta - m \sin^2 \theta + \frac{1}{2} \cos^2 \theta \gamma_{\mathbf{k}} [\sin^2 \theta (\Delta - 4n - m) + \delta] \right. \\ &\quad \left. + \cos 2\theta \gamma_{\mathbf{k}}^2 [n - \Delta \cos^2 \theta - m \sin^2 \theta] \right]\end{aligned}\quad (2.30)$$

As discussed before, angle renormalization implies changes in constant terms of  $\hat{\mathcal{H}}_2$  by an amount  $\delta A_{\mathbf{k}}$  and  $\delta B_{\mathbf{k}}$  resulting in:

$$\begin{aligned}\delta \hat{\mathcal{H}}_2 &= -\frac{H^2}{8JS^2} (n - m - \Delta) \sum_{\mathbf{k}} \left[ (1 - \gamma_{\mathbf{k}}) a_{\mathbf{k}}^\dagger a_{\mathbf{k}} - \frac{1}{2} \gamma_{\mathbf{k}} (a_{\mathbf{k}} a_{-\mathbf{k}} + a_{\mathbf{k}}^\dagger a_{-\mathbf{k}}^\dagger) \right] \\ &= -\frac{H^2 (n - m - \Delta)}{8JS^2} \sum_{\mathbf{k}} [(u_{\mathbf{k}}^2 + v_{\mathbf{k}}^2) - \gamma_{\mathbf{k}} (u_{\mathbf{k}} + v_{\mathbf{k}})^2] b_{\mathbf{k}}^\dagger b_{\mathbf{k}} + \text{"anomalous terms"}\end{aligned}$$

where the second line originates from substituting BOGOLIUBOV transformation while keeping only terms with one creation and one annihilation operator. Therefore, at the first order in

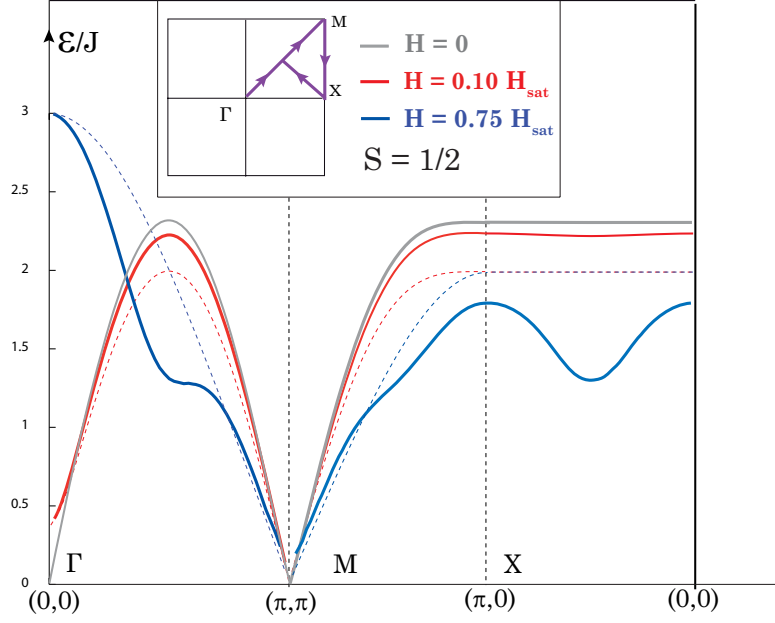


Figure 2.3: Spin 1/2 - BRILLOUIN zone plot of renormalized dispersion  $\tilde{\epsilon}_{\mathbf{k}}$  (solid lines) with corrective terms up to the  $1/S^2$  in the spin-wave expansion compared to harmonic spectrum (dashed lines). Computation of HARTREE-FOCK averages is done using a modified SIMPSON's rule on a 3000x3000 grid. Integrals in self-energy are done using a Monte-Carlo technique with  $4 \cdot 10^6$  points.

perturbation theory, the angle renormalization yields the following correction of smallness  $1/S^2$  to the dispersion relation:

$$\delta\epsilon_{\mathbf{k}}^{(2)} = \frac{H^2}{8JS^2\omega_{\mathbf{k}}}(\Delta + m - n)(1 - \gamma_{\mathbf{k}}^2 - \cos^2\theta\gamma_{\mathbf{k}}) \quad (2.31)$$

### 2.3.5 Renormalized spectrum

If contributions from the self-energy are small [10], one can substitute  $\epsilon = \epsilon_{\mathbf{k}}$  in DYSON's equation in order to get an *explicit* equation for the renormalized spectrum :

$$\tilde{\epsilon}_{\mathbf{k}} = \epsilon_{\mathbf{k}} + \delta\epsilon_{\mathbf{k}}^{(1)} + \delta\epsilon_{\mathbf{k}}^{(2)} + \Sigma_{11}^{(1)}(\mathbf{k}, \epsilon_{\mathbf{k}}) + \Sigma_{11}^{(2)}(\mathbf{k}, \epsilon_{\mathbf{k}}) \quad (2.32)$$

where  $\epsilon_{\mathbf{k}}$  is the Harmonic dispersion. A renormalized spectrum is plotted on Figure (2.3) for spin 1/2 and for different magnetic fields. For low magnetic fields, renormalization yields a moderate enhancement of the spectrum with  $|\tilde{\epsilon}_{\mathbf{k}} - \epsilon_{\mathbf{k}}| \leq 15\%$ . For greater magnetic fields, renormalization can be up to 50% so that substitution  $\epsilon = \epsilon_{\mathbf{k}}$  breaks down. The correct behavior can be recovered solving DYSON equation which implicitly define the correct spectrum [5]. Fastly growing renormalization at high field originates from growing denominator in the self-energy  $\Sigma_{11}^{(1)}$ . Around  $H = 0.75H_{sat}$  self-energy gets singular and renormalization procedure fails. This corresponds to *instability* of magnons with respect to decay processes involved in  $\Sigma_{11}^{(1)}$ . Next chapter elucidates conditions for such decays to dominate other contributions.



# Chapter 3

## Kinematics of Magnons Decay

Magnons decays originates from the existence of singularities in the self-energy involving three-particles processes. These divergencies correspond to the crossing between the one-magnon spectrum  $\epsilon_{\mathbf{k}}$  and the two-magnons continuum  $\epsilon_{\mathbf{q}} + \epsilon_{\mathbf{k}-\mathbf{q}+\mathbf{Q}}$ . In this context, this chapter aims at elucidating the conditions required for such vicinities. Analysing the momentum and energy conservation laws is sufficient to obtain decay conditions, this part therefore deals with decay *kinematics*. Decay of bosons at zero-temperature is actually a well documented problem as such phenomenon occurs in superfluid Helium-4. The following discussion is as a result adapted from early textbooks on the subject, namely from ABRIKOSOV-GORKOV-DZYALOSHINSKI's [8] and LIFSHITZ-PITAEVSKII's [7] textbooks.

### 3.1 Origin of decay

As derived in previous sections the lowest-order self-energy originating from decay processes reads :

$$\Sigma_{11}^{(1)}(\mathbf{k}, \epsilon_{\mathbf{k}}) = \frac{1}{2} \sum_{\mathbf{q}} \frac{|\Gamma_1(\mathbf{k}, \mathbf{q})|^2}{\epsilon_{\mathbf{k}} - \epsilon_{\mathbf{q}} - \epsilon_{\mathbf{k}-\mathbf{q}+\mathbf{Q}} + i0}$$

Finding the conditions for decay therefore corresponds to the computation of the roots of the following equation :

$$\epsilon_{\mathbf{k}} = \epsilon_{\mathbf{q}} + \epsilon_{\mathbf{k}-\mathbf{q}+\mathbf{Q}} \quad (3.1)$$

In the following it is assumed that equation (3.1) starts to have roots above a certain *threshold* momentum  $\mathbf{k}_c$  where it becomes possible to find at least one momentum  $\mathbf{q}$  satisfying the energy conservation. This set of threshold momenta defines the limits of the *decay region* where the one-magnon spectrum becomes unstable. On the other hand, the corresponding set of  $\mathbf{q}$ -momenta, solutions of (3.1) for a given  $\mathbf{k}$  in the decay region (or on its boundaries), define a *decay surface* where the two new magnons are created. For a given magnetic field, the decay region is unique whereas the decay surfaces depend on the chosen incoming momentum within it.

One can easily understands that at the decay threshold the right-hand side of (3.1) must be a minimum<sup>1</sup> as a function of  $\mathbf{q}$ . Expanding its right-hand side around  $\mathbf{q}^*$  yields :

$$\epsilon_{\mathbf{k}_c} = \epsilon_{\mathbf{q}^*} + \epsilon_{\mathbf{k}_c-\mathbf{q}^*+\mathbf{Q}} + (\nabla_{\mathbf{q}} \epsilon_{\mathbf{q}} - \nabla_{\mathbf{q}} \epsilon_{\mathbf{k}-\mathbf{q}+\mathbf{Q}}) \cdot \delta\mathbf{q} + \mathcal{O}(\delta\mathbf{q}^2) \quad (3.2)$$

where  $\delta\mathbf{q} = \mathbf{q} - \mathbf{q}^*$ . At the minimum, the linear term in the expansion must vanish so that created magnons have equal velocities :

$$\mathbf{v}_{\mathbf{q}^*} = \mathbf{v}_{\mathbf{k}_c-\mathbf{q}^*+\mathbf{Q}} = \mathbf{v}_2 \quad (3.3)$$

---

<sup>1</sup>Otherwise the incoming magnon momentum would be above the threshold *i.e* inside the decay region

Two different situations arise simultaneously with equation (3.3): rather one magnon is created with zero energy at the GOLDSTONE mode (section 3.2), rather both created magnons have finite energy so that the decay occurs at a given point inside the Brillouin zone (section 3.3). This classification is similar to the one found for superfluid Helium-4 where decay rather creates two excitations or a phonon. However, the excitation spectrum of Helium-4 also contains a local minimum where decay can create excitations with zero velocity, the so-called 'rotons'. Such phenomenon does not exist in the present system according to the shape of its spectrum.

## 3.2 Decay near the Goldstone mode

It is relevant to start investigating decay kinematics for particles around the GOLDSTONE mode where the spectrum is not gapped. For  $\mathbf{k} \rightarrow \mathbf{Q}$ , decay starts when  $\epsilon_{\mathbf{q}} + \epsilon_{\mathbf{k}-\mathbf{q}+\mathbf{Q}} = \epsilon_{\mathbf{q}} + \epsilon_{-\mathbf{q}}$  is minimum. Obviously, this minimum is zero and reached for  $\mathbf{q} \rightarrow \mathbf{Q}$  which implies that for both  $\mathbf{k}$  and  $\mathbf{q}$  near the GOLDSTONE mode the global minimum of  $\epsilon_{\mathbf{q}} + \epsilon_{\mathbf{k}-\mathbf{q}+\mathbf{Q}}$  is reached. As a result if decay is possible it must start at the GOLDSTONE mode.

### 3.2.1 Curvature of the spectrum

Condition for decay to start can now be formulated in terms of spectrum curvature. Assuming an isotropic system, one can expand the spectrum around the GOLDSTONE mode in the following form [8] [7] :

$$\epsilon_{\mathbf{Q}-\tilde{\mathbf{k}}} \approx v\tilde{k} + \alpha\tilde{k}^3 + \mathcal{O}(\tilde{k}^3)$$

where  $\tilde{k}$  is a small quantity. Applied to equation (3.1) this expansion yields :

$$v(\tilde{k} - \tilde{q} - |\tilde{\mathbf{k}} - \tilde{\mathbf{q}}|) = -\alpha(\tilde{k}^3 - \tilde{q}^3 - |\tilde{\mathbf{k}} - \tilde{\mathbf{q}}|^3)$$

As both  $\tilde{\mathbf{k}}$  and  $\tilde{\mathbf{q}}$  lies next to the GOLDSTONE mode, the angle  $\beta$  between their direction is small and  $|\tilde{\mathbf{k}} - \tilde{\mathbf{q}}| \approx -\frac{\tilde{k}\tilde{q}}{\tilde{k}-\tilde{q}}(1 - \cos\beta)$  with  $1 - \cos\beta > 0$ . From this expansion it finally turns out that :

$$1 - \cos\beta = 3\alpha(\tilde{k} - \tilde{q})^2 \quad (3.4)$$

and as a result, decay starts at the GOLDSTONE mode when  $\alpha > 0$ , i.e when the harmonic spectrum acquires a positive curvature. Even if this argument has been derived for an isotropic spectrum, it still holds for more complex ones provided angular dependence around the sound mode is carefully analysed.

### 3.2.2 Computation of the threshold field

In order to use the previous argument, one should expand the spectrum obtained with the linear spin-wave theory around the GOLDSTONE mode. As the actual spectrum is not isotropic correct expansions are done in the following way :

$$\gamma_k \approx -1 + \frac{\tilde{k}_x^2 + \tilde{k}_y^2}{4} - \frac{\tilde{k}_x^4 + \tilde{k}_y^4}{48} \quad \text{where } \tilde{k}_x \text{ and } \tilde{k}_y \text{ are independent variables}$$

Switching to polar coordinates defined as  $\tilde{k}_y = \tilde{k} \cos\phi$  and  $\tilde{k}_x = \tilde{k} \sin\phi$ , it is straightforward to expand the harmonic spectrum to the third order in  $\tilde{k}^3$  and obtain :

$$\epsilon_{\mathbf{Q}-\tilde{\mathbf{k}}}/4JS = \omega_{\mathbf{Q}-\tilde{\mathbf{k}}} = \left[ \frac{\cos\theta}{\sqrt{2}} \right] \tilde{k} - \left[ \frac{\cos\theta}{\sqrt{2}} \left( \frac{1 - 2\sin^2\phi \cos^2\phi}{24} + \frac{\cos 2\theta}{16 \cos^2\theta} \right) \right] \tilde{k}^3 + \mathcal{O}(\tilde{k}^3)$$

where  $\theta$  is the classical canting angle defined as  $\sin\theta = H/H_{sat}$ . It is now clear that the curvature of the spectrum explicitly depends on the magnetic field and one can define a *threshold magnetic*

field  $H^*$  above which  $\alpha$  becomes positive :

$$\frac{H^*}{H_{sat}} = \sqrt{\frac{5 - 4 \sin^2 \phi \cos^2 \phi}{8 - 4 \sin^2 \phi \cos^2 \phi}} \quad (3.5)$$

For incoming momentum sitting on the diagonal of the Brillouin zone ( $\Gamma M$  line) the threshold field is minimized and its value is:

$$H^* = \frac{2}{\sqrt{7}} H_{sat} \approx 0.76 H_{sat} \quad (3.6)$$

On the other hand, above  $H' = \sqrt{\frac{5}{8}} H_c \approx 0.79 H_{sat}$  decay occurs for any momentum close to the GOLDSTONE mode without any dependence on the angle  $\phi$ .

From the analytical considerations of this subsection, one can draw the general conclusion that decay is only possible for a field above  $\approx 76\%$  of the saturation field and first appear for magnons around the sound mode.

### 3.3 Decay within the Brillouin zone

Analysing the decay processes for any momentum inside of the Brillouin zone is far less straightforward than in the neighborhood of the GOLDSTONE mode as the decay region boundary is defined as the set of solution  $\mathbf{k}_c$  to the system :

$$\epsilon_{\mathbf{k}_c} = \epsilon_{\mathbf{k}_c - \mathbf{q} + \mathbf{Q}} + \epsilon_{\mathbf{q}} \text{ and } \frac{\partial}{\partial \mathbf{q}} [\epsilon_{\mathbf{k}_c - \mathbf{q} + \mathbf{Q}} + \epsilon_{\mathbf{q}}] = 0 \quad (3.7)$$

The second equation in (3.7) can be written more rigorously in the form :

$$\left. \frac{\partial \epsilon_{\mathbf{q}}}{\partial \mathbf{q}} \right|_{\mathbf{q}} - \left. \frac{\partial \epsilon_{\mathbf{q}}}{\partial \mathbf{q}} \right|_{\mathbf{k} - \mathbf{q} + \mathbf{Q}} = 0$$

After this transformation it is clear that the simplest way to satisfy (3.7) is to assume that created magnons have equal quasi-momenta  $q^*$ . It is obviously a very specific case and other solutions might arise while completely solving the system. Such a study is however useless as next chapter will show that the case of decay with equal momenta corresponds 'by chance' to the largest decay region. In other words, if other solutions to equations (3.7) exist, they correspond to momenta  $\mathbf{k}$  already lying inside of the 'equal momenta' decay region. Nevertheless, one should realize that this argument is not general and a complete solving might be necessary for systems with more complex spectrum [1].

#### 3.3.1 Decay in magnons with equal momenta

It is now assumed that created magnons at the threshold have equal quasi-momenta  $\mathbf{q}^*$  and  $\mathbf{q}^* + \mathbf{G}$ , where  $\mathbf{G}$  is a reciprocal lattice vector. It implies that  $\mathbf{k}_c - \mathbf{q}^* + \mathbf{Q} = \mathbf{q}^* + \mathbf{G}$  and transform equation (3.1) in the following way :

$$\epsilon_{\mathbf{k}_c} = 2\epsilon_{(\mathbf{Q} - \mathbf{k}_c)/2} \quad (3.8)$$

which gives an explicit equation for the limits of the decay region. Solutions of equation (3.8) are plotted for different magnetic fields in Figure 3.1.

As derived analytically in the previous section, decay starts at the GOLDSTONE mode and decay region rapidly spreads with increasing field. For a given magnetic field, all magnons with momentum sitting within the corresponding contour are unstable. Close to saturation, one-magnon excitations only survive next to  $\Gamma$  and  $X$  points of the Brillouin zone. When the system is saturated, all one-magnon excitations become unstable.

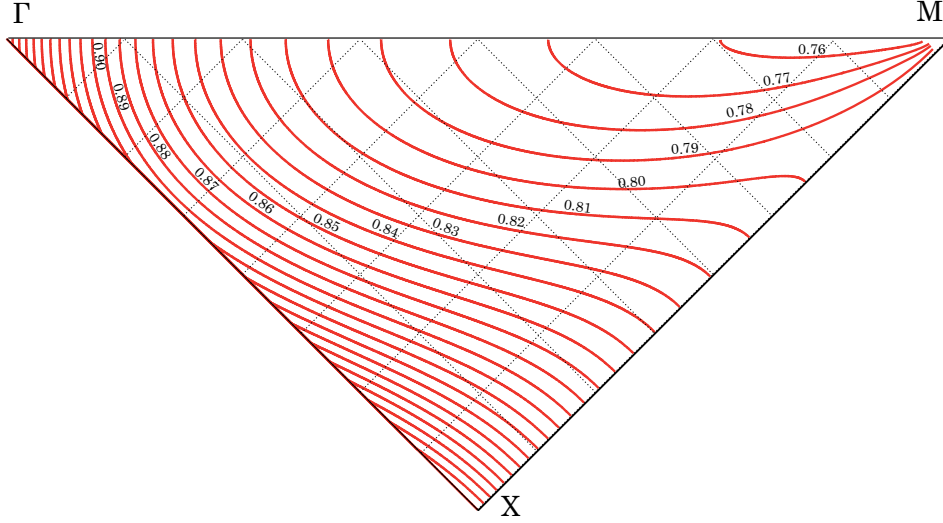


Figure 3.1: Decay region boundaries for different magnetic fields. Only 1/8 of the Brillouin zone is plotted as the whole BZ can be recovered by symmetry. Red lines stands for region boundaries. Corresponding fields are indicated on the line in fraction of the saturation field  $H_{sat}$ . Scan in field is done from  $H^*$  to  $H_{sat}$  by 1% steps. At  $H_{sat}$  the decay region is the whole Brillouin zone.

### 3.3.2 Decay surfaces

As defined previously, decay surfaces correspond to sets of momenta solutions of energy conservation for a given incoming momentum. In order to plot these surfaces, one should find, for a given  $\mathbf{k}$  within the decay region, momenta  $\mathbf{q}$  satisfying equation (3.1). Such a study can be carried out without any assumption on created magnons provided decay region is already known. Several decay surfaces are plotted in Figure 3.2 for two different incoming momenta inside of the decay region. One can easily notice that decay surfaces are always included inside of original decay region.

The most important conclusion arising from decay surfaces plots concerns the stability of created magnons. As decay surfaces remains inside the decay region, *created magnons are again unstable* with respect to two-magnons decays. As a result magnons decay has to be understood as a chain of two-magnons decay processes leading to *zero-temperature finite lifetimes excitations*.

## 3.4 Understanding decays with two-magnons density of states

A complementary approach can be carried out to understand physical reasons for decay. It will appear that two-magnons density of states has moving Van-Hove singularities that can cross the one-magnon spectrum and be therefore responsible for decays. The two-magnons density of states (DOS) for a given  $\mathbf{k}$  in the Brillouin zone and a given energy  $\epsilon$  is defined as follow :

$$\mathcal{D}_2(\mathbf{k}, \epsilon) = \sum_{\mathbf{q}} \delta(\epsilon - \epsilon_{\mathbf{q}} - \epsilon_{\mathbf{k}-\mathbf{q}+\mathbf{Q}}) = \int \frac{d^2\mathbf{q}}{(2\pi)^2} \delta(\epsilon - \epsilon_{\mathbf{q}} - \epsilon_{\mathbf{k}-\mathbf{q}+\mathbf{Q}}) \quad (3.9)$$

It is well know in condensed matter physics [16] that such an expression can be transformed in the following way :

$$\mathcal{D}_2(\mathbf{k}, \epsilon) = \frac{1}{(2\pi)^2} \oint_{\gamma(\mathbf{k}, \epsilon)} \frac{d\ell}{|\nabla_{\mathbf{q}}(\epsilon_{\mathbf{q}} + \epsilon_{\mathbf{k}-\mathbf{q}+\mathbf{Q}})|} \quad (3.10)$$

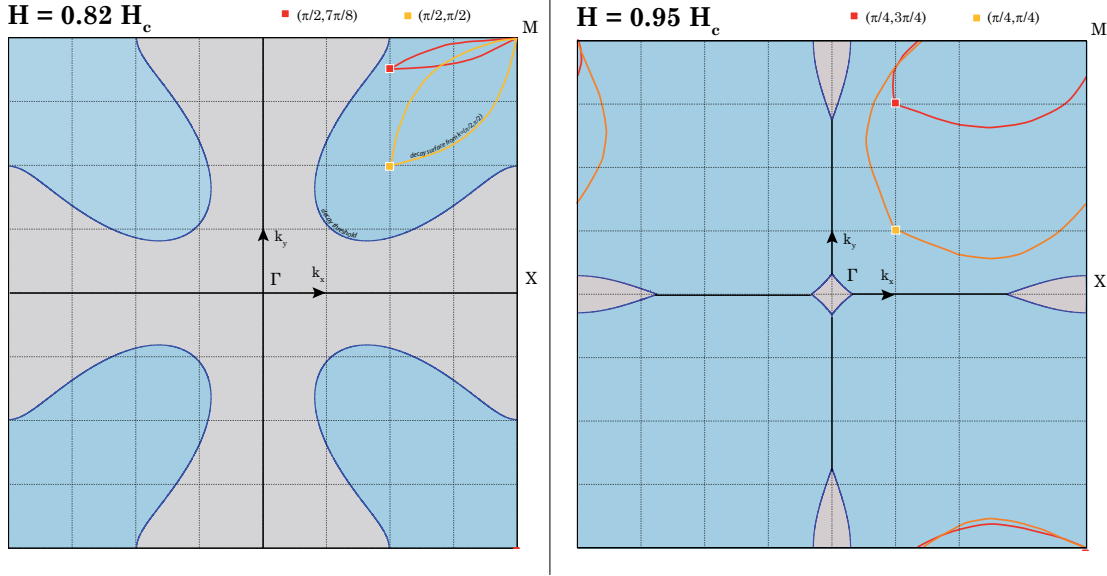


Figure 3.2: — *Left* : Decay region and two decay surfaces for  $H = 0.82H_{sat}$ . Decay region is filled in light-blue. Stable region is filled in gray. Decay surfaces corresponding to  $\mathbf{k} = (\pi/2, \pi/2)$  (respectively to  $\mathbf{k} = (\pi/2, 7\pi/8)$ ) are plotted in orange (respectively in red) — *Right* : Decay region and two decay surfaces for  $H = 0.95H_{sat}$ . Decay region is filled in light-blue. Stable region is filled in gray. Decay surfaces corresponding to  $\mathbf{k} = (\pi/4, \pi/4)$  (respectively to  $\mathbf{k} = (\pi/4, 3\pi/4)$ ) are plotted in orange (respectively in red)

where  $\gamma(\mathbf{k}, \epsilon)$  is a one-dimensional contour defined in the Brillouin zone as :

$$\gamma(\mathbf{k}, \epsilon) = \{\mathbf{q} / \epsilon_{\mathbf{q}} + \epsilon_{\mathbf{k}-\mathbf{q}+\mathbf{Q}} = \epsilon\} \quad (3.11)$$

### 3.4.1 Van-Hove singularities in the two-magnons density of states

Singularities in the two-magnon DOS appears when the integration contour defined by equation (3.11) gets close to the divergences of the integrand in equation (3.10), corresponding to the limit  $|\nabla_{\mathbf{q}}(\epsilon_{\mathbf{q}} - \epsilon_{\mathbf{k}-\mathbf{q}+\mathbf{Q}})| \rightarrow 0$ . Behavior of the two-magnon DOS can be classified according to the type of extremum, *i.e* if the two-magnons continuum has a minimum or a saddle-point. Assuming  $\mathbf{q}^*$  is an extremum of  $\epsilon_{\mathbf{q}} + \epsilon_{\mathbf{k}-\mathbf{q}+\mathbf{Q}}$  then it can be expanded as :

$$\epsilon_{\mathbf{q}} + \epsilon_{\mathbf{k}-\mathbf{q}+\mathbf{Q}} \approx \epsilon_{\mathbf{q}^*} + \epsilon_{\mathbf{k}-\mathbf{q}^*+\mathbf{Q}} + \frac{A_x}{2}(q_x - q_x^*)^2 + \frac{A_y}{2}(q_y - q_y^*)^2$$

On the one hand, if  $A_x$  and  $A_y$  have equal signs then the extremum is a local minimum corresponding to  $\epsilon_{\mathbf{q}} + \epsilon_{\mathbf{k}-\mathbf{q}+\mathbf{Q}} \approx \epsilon_c + \frac{|A|}{2}(q - q^*)^2$  and equation (3.10) reads :

$$\mathcal{D}_2(\mathbf{k}, \epsilon) \propto \int r dr \delta(\epsilon - \epsilon_c - \frac{|A|}{2}r^2) = \begin{cases} 0 & \text{if } \epsilon < \epsilon_c \\ 1 & \text{if } \epsilon > \epsilon_c \end{cases} \quad (3.12)$$

which implies a sharp jump in the two-magnons DOS while crossing this type of singular point.

On the other hand, if  $A_x$  and  $A_y$  have different signs then the extremum is a saddle-point corresponding, for  $A_x < 0$ , to  $\epsilon_{\mathbf{q}} + \epsilon_{\mathbf{k}-\mathbf{q}+\mathbf{Q}} \approx \epsilon_c - \frac{|A|}{2}(q_x - q_x^*)^2 + \frac{|A|}{2}(q_y - q_y^*)^2$  and equation (3.10) reads :

$$\mathcal{D}_2(\mathbf{k}, \epsilon) \propto \int_0^R dX \left( X^2 + \frac{\epsilon - \epsilon_c}{2|A|^2} \right)^{-1/2} \propto \ln \left[ \frac{R^2}{|\epsilon - \epsilon_c|} \right] \quad (3.13)$$

where  $R$  is a cut-off in the integration. Such a local expression for the two-magnons DOS is characteristic of symmetric logarithmic singularities.

As a result from analytical considerations, Van-Hove singularities in the two-magnons DOS appear rather in the form of *sharp asymmetric jumps*, rather in the form of *symmetric logarithmic divergences*. Such behavior is represented on Figure 3.5 where the upper-part represents both the gradient of the two-magnons continuum and the integration contour of equation (3.11) and the lower-part the resulting shape of the two-magnons DOS. It is clear that singularities originate from reduced distance between integration contour and gradient zeros. Therefore, number of Van-Hove singularities can be fully understood with equation (3.10). Knowledge on their positions arise while comparing with  $\epsilon$ -dependent integration contours. Finally, shape of singularities depends on nature of the two-magnons continuum near its extrema.

### 3.4.2 Evolution of the density of states with magnetic field

Two-magnons DOS undergoes major changes while increasing applied magnetic field. This evolution concerns both peaks position and shape. Decay become possible while singularities of the two-magnons DOS cross the one-magnon one. In this regime, two-magnons excitations have lower energy than one-magnon ones.

Below threshold, two-magnons excitations only exist above a certain energy corresponding to the one-magnon spectrum. Density of states linearly increase next to this point so that singularities only lies at higher energies (Figure 3.4). With increasing magnetic field, singularities move along the energy axis so that two-magnons DOS is non-zero on a broader range of energy (Figure 3.5—*upper-right*).

When magnetic field approaches its threshold value and while incoming momentum  $\mathbf{k}$  is fixed, a logarithmic divergence gets closer and closer to the one-magnon energy (Figure 3.5—*main*). In the meantime, as harmonic spectrum acquire a positive curvature at the decay threshold, one of the component of  $\nabla_{\mathbf{q}}(\epsilon_{\mathbf{q}} + \epsilon_{\mathbf{k}-\mathbf{q}+\mathbf{Q}})$  changes sign. As a result, decay corresponds to logarithmic peak of the two-magnons DOS crossing the one-magnon spectrum while transforming into a 'sharp jump' like peak. As this singularity continue its way down in energy when magnetic field increases from threshold to saturation, two-magnons excitations have a significative and relatively flat density of states, below the one-magnon energy. Therefore, kinematics of decay can be fully understood with properties of two-magnons density of states.

As a conclusion to this chapter, it is useful to emphasize its most important results. Decay first appears at the GOLDSTONE mode when magnetic field reaches 76% of the saturation field. While field increases, decay region spreads in the Brillouin zone so that all one-magnon excitations become unstable at the saturation. Moreover, decay corresponds to the existence of Van-Hove singularities in the two-magnons continuum at lower energy than one-magnon excitations. New magnons originating from decay are created within the original decay region so that they are again unstable. As a result, this problem has to be treated as a multi-decay process where excitations acquire finite lifetimes. Next chapter about decay dynamics aims at studying such multi-decay processes.

$H = 0.10 H_c$       ■  $\mathbf{k}=(7\pi/8,\pi/4)$       M

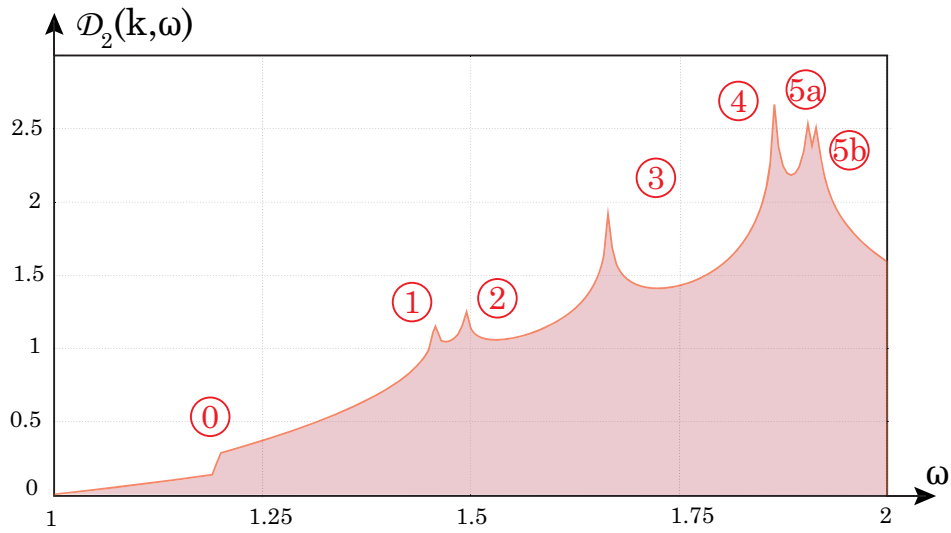
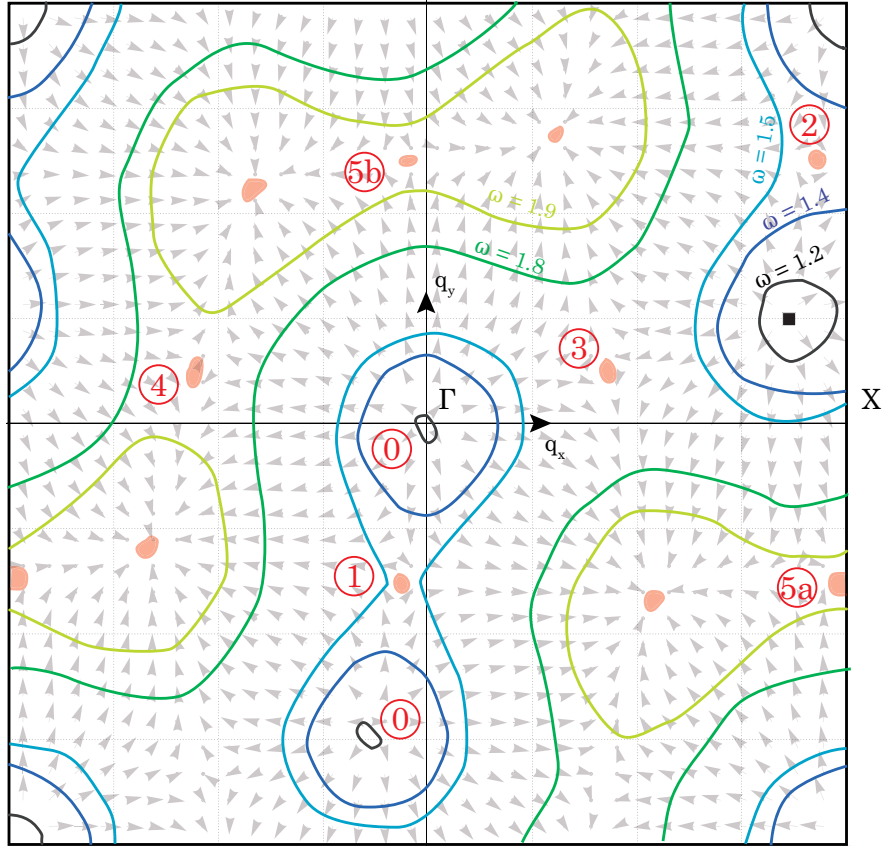


Figure 3.3: Magnetic field is fixed to  $0.10H_{sat}$  and  $\omega$  is dimensionless energy ( $\epsilon = 4JS\omega$ ) — *Up* : Brillouin zone with  $\nabla_{\mathbf{q}}(\omega_{\mathbf{q}} + \omega_{\mathbf{k}-\mathbf{q}+\mathbf{Q}})$  for  $\mathbf{k} = (7\pi/8, \pi/4)$  represented with gray arrows and  $\gamma(\mathbf{k}, \omega)$  represented with color lines for several values of  $\omega$ . Saddle-points are designed with red dots. — *Down* : The two-magnons DOS for corresponding  $\mathbf{k}$ . Singularities are related to points of the Brillouin-zone they originate from. The DOS is zero out of the displayed  $\omega$  scale.

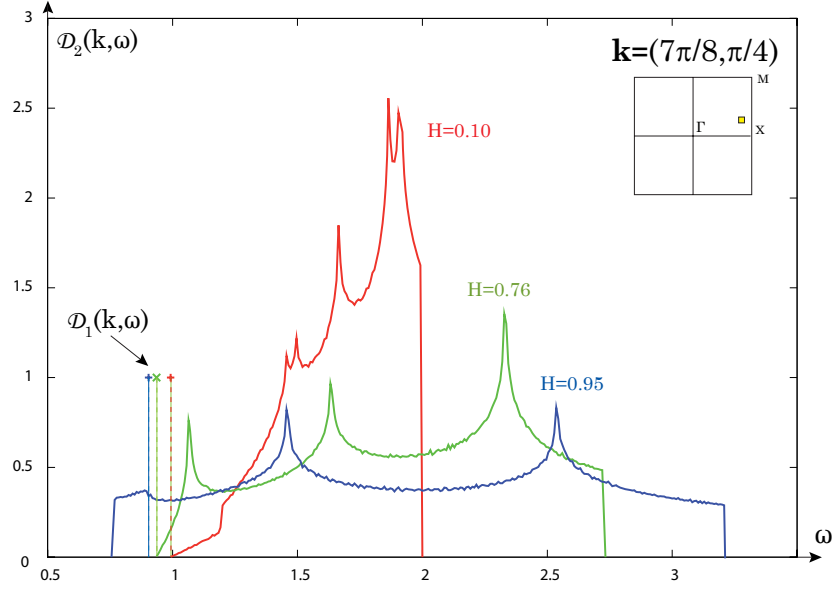


Figure 3.4: Numerical integration of equation (3.9) with 2D Monte-Carlo technique. Incoming momentum  $\mathbf{k} = (7\pi/8, \pi/4)$  is chosen off diagonal. Solid lines represent two-magnons DOS for three different magnetic field. Dashed lines represent the corresponding one-magnon DOS

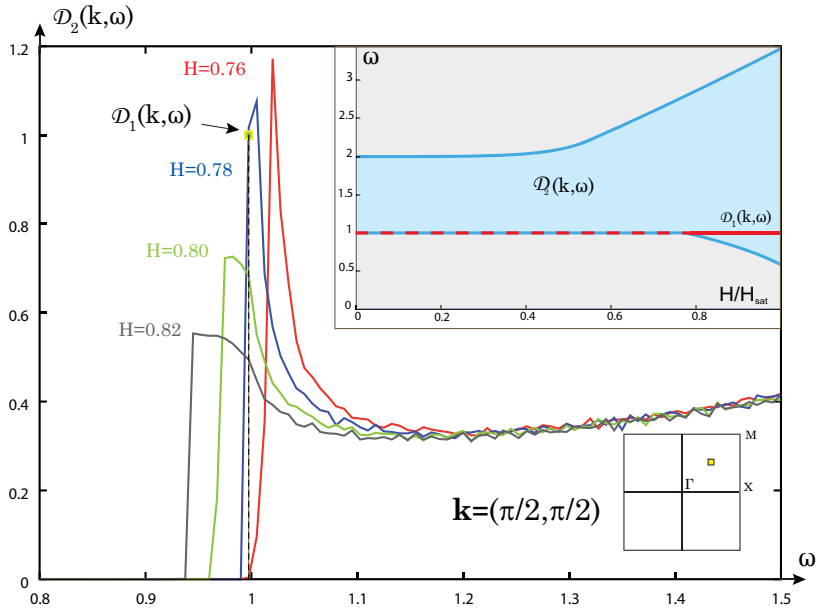


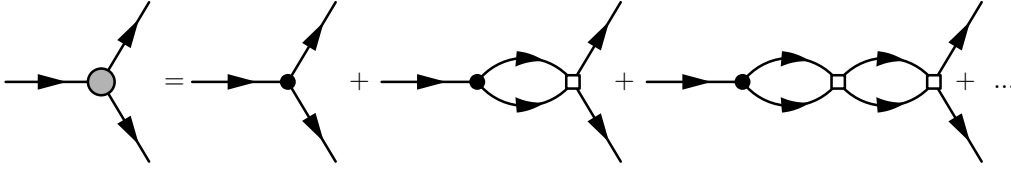
Figure 3.5: —*Main figure* : Numerical integration of equation (3.9) with 2D Monte-Carlo technique. Incoming momentum  $\mathbf{k} = (\pi/2, \pi/2)$  is chosen on the diagonal. Solid lines represent two-magnons DOS for several magnetic field around threshold. Dashed line represents the one-magnon DOS which is field-independent for this  $\mathbf{k}$  — *Upper-right figure* : Non-zero region for two-magnons DOS is filled in light-blue and plotted versus increasing magnetic field. Red line stands for the position of the one-magnon DOS



# Chapter 4

## Decay Dynamics

Previous considerations about kinematics of magnons decay led to important results. Among them, the existence of a threshold magnetic field is of considerable experimental interest. However, singularities in the self energy does not make physical sense. Condensed-matter physicists are used to deal with such problems, for example when computing the ground state of interacting electronic gas in a solid. In this case, perturbative expansions can be made consistent using the so-called 'Random Phase Approximation' infinite sum. In the same spirit, divergencies in bosonic systems with decays such as superfluid Helium-4, are removed by transformation of simple vertices in the following 'ladder series' [7]:



where black dot stands for first-order decay vertex and white square stands for first-order two-particle scattering vertex.

Nevertheless, as magnons resulting from decay are unstable, divergencies can be removed in an *alternative way*, namely with the introduction of *imaginary self-energy*. In this context, interacting magnons are believe to acquire finite lifetime, whereas their spectrum is weakly renormalized by interactions. This chapter therefore aims at showing how magnons lifetimes lift divergencies. Furthermore, as directly related to experimentally accessible datas, magnons lifetimes are calculated within the framework of the *self-consistent Born approximation (SCBA)*.

### 4.1 A closer look at singularities

#### 4.1.1 Analytical properties of the Self-energy near divergences

Near the decay threshold one can expand the two magnons continuum in powers of  $k$  and  $q$  like:

$$\epsilon_{\mathbf{q}} + \epsilon_{\mathbf{k}-\mathbf{q}+\mathbf{Q}} \approx \epsilon_c + v(k - k_c) + \alpha_x (q_x - q_x^*)^2 + \alpha_y (q_y - q_y^*)^2 + \mathcal{O}(k^2) + \mathcal{O}(q^2) \quad (4.1)$$

As shown before, singularities appear in the self-energy when the two-magnon continuum has rather a local minimum or a saddle-point. The singular self-energy then reads :

$$\Sigma_{11,\pm}^{(1)}(\mathbf{k}, \epsilon) = \frac{1}{8\pi^2} \int \frac{dq_x dq_y |\Gamma_1(\mathbf{k}, \mathbf{q})|^2}{\epsilon - \epsilon_c - v(k - k_c) - |\alpha_x| (q_x - q_x^*)^2 \pm |\alpha_y| (q_y - q_y^*)^2 + i0} \quad (4.2)$$

where minus sign (-) in front of  $|\alpha_y|$  corresponds to minimum and plus sign (+) corresponds to saddle-point. The analytical properties of (4.2) are only determined by its singularities so that

the vertex part can be approximate as its average value  $\Gamma_1$  and finite c-numbers can be neglected so that :

$$\Sigma_{11,\pm}^{(1)}(\mathbf{k}, \epsilon) \propto \Gamma_1^2 \int \frac{d\tilde{q}_x d\tilde{q}_y}{\Delta\epsilon - v\Delta k + i0 - |\alpha_x| \tilde{q}_x^2 \pm |\alpha_y| \tilde{q}_y^2} = \frac{\Gamma_1^2}{\sqrt{|\alpha_x| |\alpha_y|}} \int \frac{dudv}{z - u^2 \pm v^2} \quad (4.3)$$

where  $\tilde{q}_x = q_x - q_x^*$ ,  $\tilde{q}_y = q_y - q_y^*$ ,  $\Delta\epsilon = \epsilon - \epsilon_c$ ,  $\Delta k = k - k_c$ ,  $u = \tilde{q}_x \sqrt{|\alpha_x|}$ ,  $v = \tilde{q}_y \sqrt{|\alpha_y|}$  and  $z = \Delta\epsilon - v\Delta k + i0$ .

The behavior of (4.3) is fully determined near the singularities by the properties of the integrals  $I_+(z)$  and  $I_-(z)$  which can be defined for  $\text{Re}(z) > 0$  as<sup>1</sup> :

$$I_{\pm}(z) = \int_{-\infty}^{\infty} du \int_{-\infty}^{\infty} \frac{dv}{\pm v^2 + [\text{Re}z - u^2] + i\text{Im}z} \quad (4.4)$$

In the case of  $I_+(z)$  The integral on  $v$  can be computed by splitting the integration domain while carefully checking the positions of residues. If  $u^2 > \text{Re}z$  then the residues are in  $v^* = \pm\sqrt{u^2 - z}$ , whereas if  $u^2 < \text{Re}z$  the residues lies in  $v^* = \pm i\sqrt{z - u^2}$ . Closing the contour in the upper half plane yields :

$$I_+(z) = \int_{-\infty}^{\infty} du \frac{2i\pi}{2v^*} = 2\pi \int_0^{\sqrt{\text{Re}z}} \frac{du}{\sqrt{z - u^2}} - 2i\pi \int_{\sqrt{\text{Re}z}}^{\infty} \frac{du}{\sqrt{u^2 - z}}$$

The first integral in (4.4) cannot be computed analytically and reads :

$$I_{+,1}(z) = 2\pi \int_0^1 \frac{du'}{\sqrt{1 - u'^2 + i\frac{\text{Im}z}{\text{Re}z}}}$$

whereas the second integral can be expressed analytically provided the integration on  $u$  is cut-off at a given  $R$  :

$$I_{+,2}(z) = -2i\pi \ln \left( u + \sqrt{u^2 - z} \right) \Big|_{\sqrt{\text{Re}z}}^R \rightarrow -2i\pi \ln \left[ \frac{2R}{\sqrt{\text{Re}z} + e^{-i\pi/4} \sqrt{\text{Im}z}} \right]$$

When  $\text{Re}(z) < 0$  the integration on  $u$  in (4.4) is carried out before integration on  $v$  so that the integral  $I_{+,1}(z)$  changes sign. However, choosing a different pole in the upper half-plane prevent the sign of  $I_{+,2}(z)$  to change.

With the same analysis as for  $I_+(z)$ , one can obtain :

$$I_-(z) = 2\pi \left( \ln \left[ \frac{\sqrt{\text{Re}^2 z + \text{Im}^2 z}}{R} \right] - i \left[ \frac{\pi}{2} + \arctan \frac{\text{Re}z}{\text{Im}z} \right] \right)$$

As a result, and in the limit  $\text{Im}z \rightarrow 0^+$  :

$$\Sigma_{11,+}^{(1)}(\mathbf{k}, \epsilon) \propto \Gamma_1^2 \frac{\pi}{2} + i\Gamma_1^2 \ln \left[ \frac{|\Delta\epsilon - v_c \Delta k|}{R} \right] \quad \text{and} \quad \Sigma_{11,-}^{(1)}(\mathbf{k}, \epsilon) \propto \Gamma_1^2 \ln \left[ \frac{|\Delta\epsilon - v_c \Delta k|}{R} \right] - i\Gamma_1^2 \pi \quad (4.5)$$

One can conclude from this analytical considerations, that logarithmic singularities appear in the *real part* of the self-energy near a local minimum whereas such divergence occurs in its *imaginary part* near a saddle-point. As singularities responsible for decays always transform to a local minimum when threshold is crossed,  $\Sigma_{11,-}^{(1)}(\mathbf{k}, \epsilon)$  is the most interesting quantity.

---

<sup>1</sup> $\text{Im}(z)$  is taken positive by definition of the retarded Green's function involved in the self-energy expression

### 4.1.2 Finite lifetimes remove divergences

Imaginary part of  $z$  is *a priori* introduced to shift poles of the Green's function from the real axis so as to perform Fourier transform but sent to zero in the end. However, one can check that introducing a finite imaginary part  $\text{Im}(z) = \Lambda$  removes divergences in the self-energy. For this purpose it is convenient to write  $z$  in polar coordinates as  $z = r e^{i\phi}$  with  $\phi$  restricted to interval  $[0, \pi/2]$  (respectively  $[\pi/2, \pi]$ ) by the condition  $\text{Re}z > 0$  (respectively  $\text{Re}z < 0$ ).

In the limit  $\phi \rightarrow \tilde{\phi}$ , corresponding to small imaginary part, a straightforward Taylor expansion for  $I_{+,1}(z)$  gives  $I_{+,1}(z) \approx \pi/2 - i\tilde{\phi} \int_0^1 du' (1-u')^{-1}$  which is ill-defined as the integral diverges. Such problems in taking limits already arose in the calculation of the magnetization curve of such a system [20]. Using MATHEMATICA, the correct behavior can be computed as  $I_1(z) \approx \pi/2 - e^{-i\pi/4} \sqrt{\tilde{\phi}}$  so that in this limit the self-energy becomes :

$$\Sigma_{11,+}^{(1)}(\mathbf{k}, \epsilon) \propto \Gamma_1^2 \left[ \pi/2 - e^{-i\pi/4} \sqrt{\tilde{\phi}} + i \ln \frac{r}{R} \right]$$

Going back to time dependent picture, it is well-know that finite imaginary part leads to a factor  $e^{\Lambda t}$  in the expression of magnons Green's function. As a result, the quantity  $\Lambda$  is physically understood as a *decay rate*. In this spirit, when decay rate is non-zero, magnons acquire finite lifetimes and self-energy becomes :

$$\Sigma_{11,+}^{(1)}(\mathbf{k}, \epsilon) \propto \Gamma_1^2 \left( \pi/2 - e^{-i\pi/4} \sqrt{\arctan \frac{\Lambda}{\Delta\epsilon - v_c \Delta k}} \right) + i\Gamma_1^2 \ln \left[ \frac{\sqrt{(\Delta\epsilon - v_c \Delta k)^2 + \Lambda^2}}{R} \right] \quad (4.6)$$

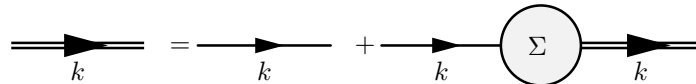
$$\Sigma_{11,-}(\mathbf{k}, \epsilon) \propto \Gamma_1^2 \ln \left[ \frac{\sqrt{(\Delta\epsilon - v_c \Delta k)^2 + \Lambda^2}}{R} \right] - i\Gamma_1^2 \left( \frac{\pi}{2} + \arctan \frac{\Delta\epsilon - v_c \Delta k}{\Lambda} \right) \quad (4.7)$$

It is clear that even small decay rates completely removes divergences in the self-energy. The following analysis will be devoted to the explicit computation of magnons decay rates within the self-consistent Born approximation.

## 4.2 Analytical expressions for magnons decay rates

### 4.2.1 The Self-Consistent Born Approximation

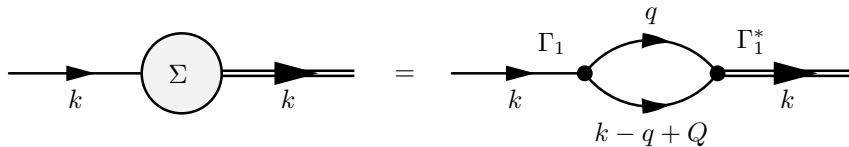
At this level of the dissertation, and in order to be aware of approximations used, it is useful to remember the expression for DYSON's equation:



$$\text{Double line } k = \text{Single line } k + \text{Single line } k \text{ --- } \Sigma \text{ --- Double line } k \quad (4.8)$$

where thin lines correspond to *unperturbed* GREEN's functions ( $\mathcal{G}^o(\mathbf{k}, \epsilon)^{-1} = \epsilon - \epsilon_k + i\delta$ ) and double ones to *full* GREEN's functions ( $\mathcal{G}(\mathbf{k}, \epsilon)^{-1} = \mathcal{G}^o(\mathbf{k}, \epsilon)^{-1} - \Sigma(\mathbf{k}, \epsilon)$ ).

Lowest order decay processes originates from  $\Sigma_{11}^{(1)}$  and this study first concentrated on such a one-loop self-energy giving explicit form of the full magnon GREEN's function:

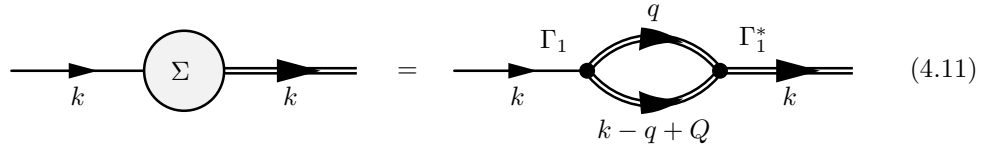


$$\text{Single line } k \text{ --- } \Sigma \text{ --- Double line } k = \text{Single line } k \text{ --- } \Gamma_1 \text{ --- Loop --- } \Gamma_1^* \text{ --- Double line } k \quad (4.9)$$

Even if kinematics condition for decay were derived in such a framework it appeared that it is necessary to go beyond this model in order to include multi-decay processes. This first order decay model actually corresponds to approximation scheme known as the *Born Approximation* (BA). In this context the self-energy is already known and reads:

$$\begin{aligned}\Sigma_{11}^{BA}(\mathbf{k}, \epsilon) &= \frac{i}{2} \sum_{\mathbf{q}} \int \frac{d\epsilon'}{2\pi} |\Gamma(\mathbf{k}, \mathbf{q})|^2 \mathcal{G}^o(\mathbf{k}, \epsilon') \mathcal{G}^o(\mathbf{k} - \mathbf{q} + \mathbf{Q}, \epsilon - \epsilon') \\ &= -\frac{1}{2} \sum_{\mathbf{q}} \frac{|\Gamma_1(\mathbf{k}, \mathbf{q})|^2}{\epsilon - \epsilon_{\mathbf{q}} - \epsilon_{\mathbf{k}-\mathbf{q}+\mathbf{Q}} + i0^+}\end{aligned}\quad (4.10)$$

One way to go beyond this approximation consists in substituting unperturbed GREEN's function with full GREEN's function in the self-energy. Dressed lines in the diagram allow multiple decay processes and yields :

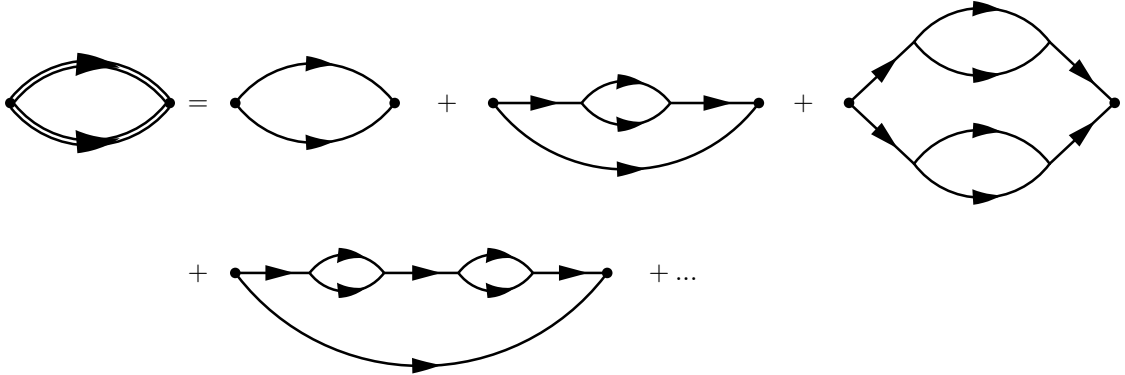


$$(4.11)$$

This method is known as the *Self-Consistent Born Approximation* (SCBA) [11]. Using DYSON's equation the self-energy yields :

$$\begin{aligned}\Sigma_{11}^{SCBA}(\mathbf{k}, \epsilon) &= \frac{i}{2} \sum_{\mathbf{q}} \int \frac{d\epsilon'}{2\pi} |\Gamma(\mathbf{k}, \mathbf{q})|^2 \mathcal{G}(\mathbf{k}, \epsilon') \mathcal{G}(\mathbf{k} - \mathbf{q} + \mathbf{Q}, \epsilon - \epsilon') \\ &= \frac{i}{2} \sum_{\mathbf{q}} \int \frac{d\epsilon'}{2\pi} \frac{|\Gamma(\mathbf{k}, \mathbf{q})|^2}{\left[ \epsilon' - \epsilon_{\mathbf{q}} - \Sigma_{11}^{(1)}(\mathbf{q}, \epsilon') \right] \left[ \epsilon - \epsilon' - \epsilon_{\mathbf{k}-\mathbf{q}+\mathbf{Q}} - \Sigma_{11}^{(1)}(\mathbf{k} - \mathbf{q} + \mathbf{Q}, \epsilon - \epsilon') \right]}\end{aligned}\quad (4.12)$$

The SCBA is a non-perturbative approach in the sense that it corresponds to summing up an infinite series of self-energies. The  $n$ -th term of this series corresponds to the sum of all topologically different self-energies with  $n$  loops of unperturbed lines. In a very schematical point of view this method corresponds to such a series :



#### 4.2.2 Magnons decay rates within the SCBA

Magnons with finite lifetimes have a spectrum which is solution of the following equation:

$$\epsilon = \epsilon_{\mathbf{k}}^o + \text{Re}[\Sigma(\mathbf{k}, \epsilon)] + i\Lambda(\mathbf{k}, \epsilon)$$

with  $\epsilon_{\mathbf{k}}^o$  the harmonic spectrum and  $\epsilon$  the renormalized one.

Spin-wave theory within the HOLSTEIN-PRIMAKOFF framework only gives consistent results when *all the contributions* to a given  $1/S$  order are summed up. If it is not the case, the theory is likely to fail at the GOLDSTONE mode predicting a gapped spectrum. In the SCBA, self-energies are combined such as the GREEN's function contain terms of any order in the  $1/S$  expansion. On the other hand, at the  $1/S^1$  order, decay processes only originates from  $\Sigma_{11}^{(1)}$  and other contribution to the self-energy at this order are forgotten. As a result, it is hopeless to compute a renormalized spectrum in the SCBA as expansion to all orders is only done for one chosen term. In order to keep the spectrum gapped while computing decay rates, real part of the self-energy has to be neglected and the harmonic spectrum used. Furthermore, higher order contributions that might introduce other decay processes are not taken in account. Selecting the appropriate terms yields :

$$\epsilon = \epsilon_{\mathbf{k}}^o + i\Lambda(\mathbf{k}, \epsilon) \text{ with } \Lambda(\mathbf{k}, \epsilon) = \frac{1}{S}\tilde{\Lambda}^{(1)} + \frac{1}{S^2}\tilde{\Lambda}^{(2)} + \dots$$

It is also necessary to restrict the study to "on-shell" processes where energy conservation is forced at each vertex. In this regime  $\Lambda(\mathbf{k}, \epsilon) = \Lambda(\mathbf{k}, \epsilon_{\mathbf{k}}^o) \equiv \Lambda_{\mathbf{k}}$  which is not explicitly energy-dependent. It follows that one can carry out the integration in (4.12) with respect to  $\epsilon'$  by closing the contour in the upper-half plane :

$$\Sigma_{11}^{SCBA}(\mathbf{k}, \epsilon_{\mathbf{k}}^o) = \frac{1}{2} \sum_{\mathbf{q}} \frac{\Gamma(\mathbf{k}, \mathbf{q})^2}{\epsilon_{\mathbf{k}}^o - \epsilon_{\mathbf{q}}^o - \epsilon_{\mathbf{k}-\mathbf{q}+\mathbf{Q}}^o - i[\Lambda_{\mathbf{q}} + \Lambda_{\mathbf{k}-\mathbf{q}+\mathbf{Q}}]} \quad (4.13)$$

Going to the imaginary part of equation (4.13) one can finally derive the expression for magnons decay rates within the self-consistent Born approximation :

$$\Lambda_{\mathbf{k}} = \frac{1}{2} \sum_{\mathbf{q}} \frac{\Gamma(\mathbf{k}, \mathbf{q})^2 [\Lambda_{\mathbf{q}} + \Lambda_{\mathbf{k}-\mathbf{q}+\mathbf{Q}}]}{[\epsilon_{\mathbf{k}}^o - \epsilon_{\mathbf{q}}^o - \epsilon_{\mathbf{k}-\mathbf{q}+\mathbf{Q}}^o]^2 + [\Lambda_{\mathbf{q}} + \Lambda_{\mathbf{k}-\mathbf{q}+\mathbf{Q}}]^2} \quad (4.14)$$

The last step is to transform this expression in a normalized one using  $\epsilon_{\mathbf{q}}^o = 4JS\omega_{\mathbf{q}}$  and  $\Lambda_{\mathbf{q}} = 4JS\lambda_{\mathbf{q}}$  where  $\omega$  and  $\lambda$  are dimensionless. Recalling that  $\Gamma(\mathbf{k}, \mathbf{q}) = -\tilde{\Gamma}(\mathbf{k}, \mathbf{q})H_c \cos\theta \sin\theta/\sqrt{2S}$  it is finally possible to write :

$$\lambda_{\mathbf{k}} = \frac{\cos^2\theta \sin^2\theta}{S} \sum_{\mathbf{q}} \frac{\tilde{\Gamma}(\mathbf{k}, \mathbf{q})^2 [\lambda_{\mathbf{q}} + \lambda_{\mathbf{k}-\mathbf{q}+\mathbf{Q}}]}{[\omega_{\mathbf{k}} - \omega_{\mathbf{q}} - \omega_{\mathbf{k}-\mathbf{q}+\mathbf{Q}}]^2 + [\lambda_{\mathbf{q}} + \lambda_{\mathbf{k}-\mathbf{q}+\mathbf{Q}}]^2} \quad (4.15)$$

It is important to notice that dimensionless decay rate explicitly depends on the value of S. As equation (4.15) is non linear, results for different spins are expected to change in a non-trivial way.

### 4.3 Numerical integration of self-consistent equations

In order to integrate equation numerically (4.15) one should assume it converges toward a fixed point. In this case, self-consistent equation is solved step by step, starting from an initial distribution of  $\lambda$ 's. Initial decay rates are denoted  $\lambda^o$  and are only introduced so as to avoid division by zero. They can be chosen arbitrary small (within the machine precision) but for the purpose of numerical integration it is convenient to choose a value  $\delta \approx 10^{-3}$ . Iterations to be done corresponds to the following algorithm :

$$\begin{cases} \lambda_{\mathbf{k}}^{(0)} = \delta \\ \lambda_{\mathbf{k}}^{(1)} = \frac{\cos^2\theta \sin^2\theta}{S} \sum_{\mathbf{q}} \frac{\tilde{\Gamma}(\mathbf{k}, \mathbf{q})^2 [\lambda_{\mathbf{q}}^{(0)} + \lambda_{\mathbf{k}-\mathbf{q}+\mathbf{Q}}^{(0)}]}{[\omega_{\mathbf{k}} - \omega_{\mathbf{q}} - \omega_{\mathbf{k}-\mathbf{q}+\mathbf{Q}}]^2 + [\lambda_{\mathbf{q}}^{(0)} + \lambda_{\mathbf{k}-\mathbf{q}+\mathbf{Q}}^{(0)}]^2} \\ \lambda_{\mathbf{k}}^{(2)} = \dots \end{cases}$$

Born approximation corresponds to *one* iteration in the previously depicted algorithm. Distribution of  $\lambda^{(1)}$ 's (Figure 4.1) for  $H = 0.82H_{sat}$  and  $H = 0.95H_{sat}$  can be fruitfully compared with previously estimated decay regions (Figure 3.2). As region where  $\lambda$ 's are not zero perfectly overlaps them, initial guess on their shape was right. Largest decay regions for a given magnetic field corresponds to decay in magnons with equal momenta. Near divergences of the two-magnons DOS, decay rates grows fastly as guessed from analytical considerations on singularities. Therefore, in the BA, borders between decaying and non-decaying region are well-defined : decay rates sharply jumps from zero to a significative value. One should also notice that decay rates are small both in the center of the Brillouin zone ( $\mathbf{k} \rightarrow 0$ ) and near antiferromagnetic ordering vector ( $\mathbf{k} \rightarrow \mathbf{Q}$ ). As collective precession of the spins around magnetic field direction are believed to remain unchanged by quantum fluctuations [5], damping due to decay should also vanish in the zone center. Near the GOLDSTONE mode, one can analytically check that decay rates smoothly go to zero due to behavior of the vertex part.

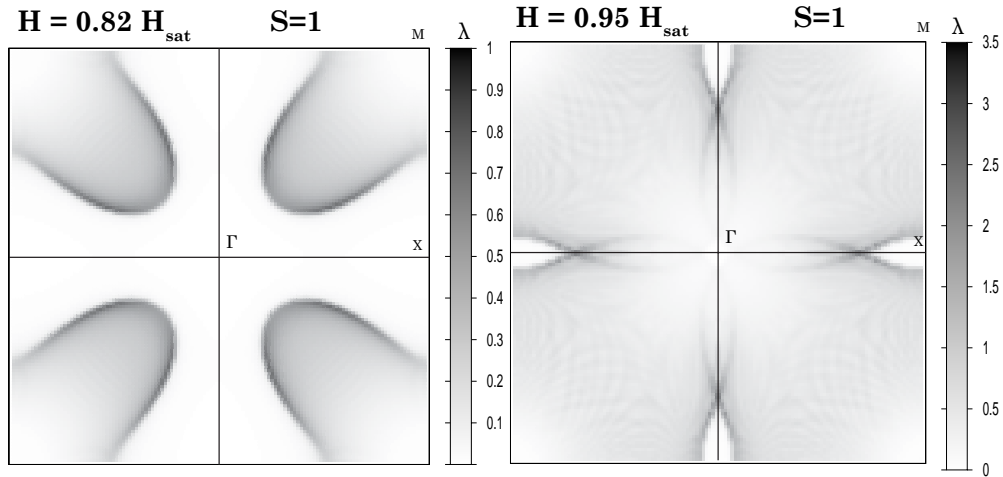


Figure 4.1: Intensity plot in the Brillouin zone of magnons decay rates within the Born approximation. Darkest regions correspond to largest dimensionless decay rates

Problems arise while performing self-consistent algorithm, as simple routines return rapidly growing decay rate near the GOLDSTONE mode. This is identified as numerical hits on singular points of the vertex part. It is possible expand the vertex as :

$$\tilde{\Gamma}_1(\mathbf{k}, \mathbf{q}) \propto -\frac{1}{\sqrt{\tilde{k}\tilde{q}(\tilde{k}-\tilde{q})}} \left[ \tilde{q} - \tilde{k} + |\tilde{\mathbf{k}} - \tilde{\mathbf{q}}| + \mu\tilde{k}\tilde{q}(\tilde{k} - \tilde{q}) \right] \quad (4.16)$$

where  $\tilde{\mathbf{k}} = \mathbf{k} - \mathbf{Q}$ ,  $\tilde{\mathbf{q}} = \mathbf{q} - \mathbf{Q}$ , and  $\mu$  is a c-number. Decay rates therefore goes to zero at the GOLDSTONE mode following a cubic power law [5] which is not consistent with first numerical tests. One therefore needs to go beyond a 'simple-minded' numerical procedure.

Numerical computation of decay rates is done using a gridded Brillouin zone where values of  $\lambda$  are tabulated and re-computed at each iteration. On this grid, quantities  $\tilde{k}$  and  $\tilde{q}$  take discrete values so that quantity  $\tilde{q} - \tilde{k} + |\tilde{\mathbf{k}} - \tilde{\mathbf{q}}|$  do not get smoothly to zero and do not compensate increasing values of  $\tilde{k}\tilde{q}(\tilde{k}-\tilde{q})$ . As a result values for  $\lambda$ 's have to be interpolated on a refined mesh. The resulting algorithm uses a sparse  $\mathbf{k}$ -grid where  $\lambda_{\mathbf{k}}$  values are computed using integration on a much more precise  $\mathbf{q}$ -grid. Values of  $\lambda$ 's on this new grid are computed with a bicubic interpolation. As external  $\mathbf{k}$  remains far away from the GOLDSTONE mode, integration can be done on a smooth function of  $\mathbf{q}$  and the cubic behavior is recovered.

Typical results for decay rates are presented below for  $S = 1/2$ ,  $S = 1$  and  $S = 5/2$  (Figure 4.2 and Figure 4.3). Self-consistent procedure rapidly converges so that 10 iterations are sufficient to get an good average precision :  $N_k^{-2} \sum_k |\lambda_k^{(n)} - \lambda_k^{(n-1)}| < 10^{-6}$  for  $n = 10$ . Introducing a

significant imaginary part in the self-energy not only remove its divergences but spreads the decay region to the whole Brillouin zone. Sharp jumps between decaying and non decaying regions, depicted in the BA, are strongly blurred so that in the SCBA *all magnons acquire finite lifetime* above threshold. As in the BA, excitations in the center of the Brillouin and at the GOLDSTONE mode zone remains well defined. However, for  $H^* < H < 0.90H_{sat}$  magnons damping is significant around the middle of  $\Gamma$ M lines whereas close to saturation and for  $0.90H_{sat} < H < 0.99H_{sat}$  strong damping moves to the middle of  $\Gamma$ X lines. Going from spin 1 to spin 5/2 non-uniformly reduces values of decay rates by a factor  $\approx 2$ .

As a conclusion from this chapter, one should remember that introducing significant decay rates removes divergences so that all magnons start to decay above the threshold field. Contribution from imaginary part of the self-energy are believed to be the dominant effects of interactions so that an harmonic description of the spectrum have been used. In such an approximation, magnons are strongly damped in large portions of the BRILLOUIN. Spectrum line width can be experimentally studied with neutron scattering techniques. It is the aim of next chapter to relate theoretical knowledge on decay rates to observable neutron scattering cross sections. Hopefully, as neutrons are weakly interacting probes, computation of first-order spin correlations within the linear response theory is of reasonable accuracy.

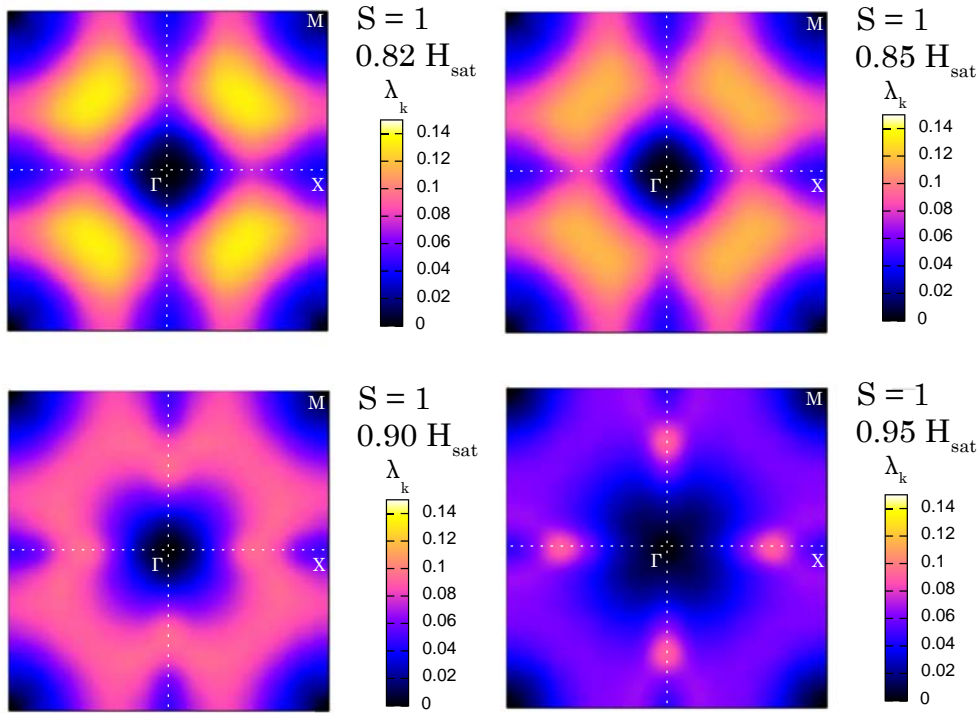


Figure 4.2: Intensity plot in the Brillouin zone of magnons decay rates within the SCBA for spin 1. Values for  $\lambda$  are computed on a 12x12 grid and interpolated on a 600x600 grid.

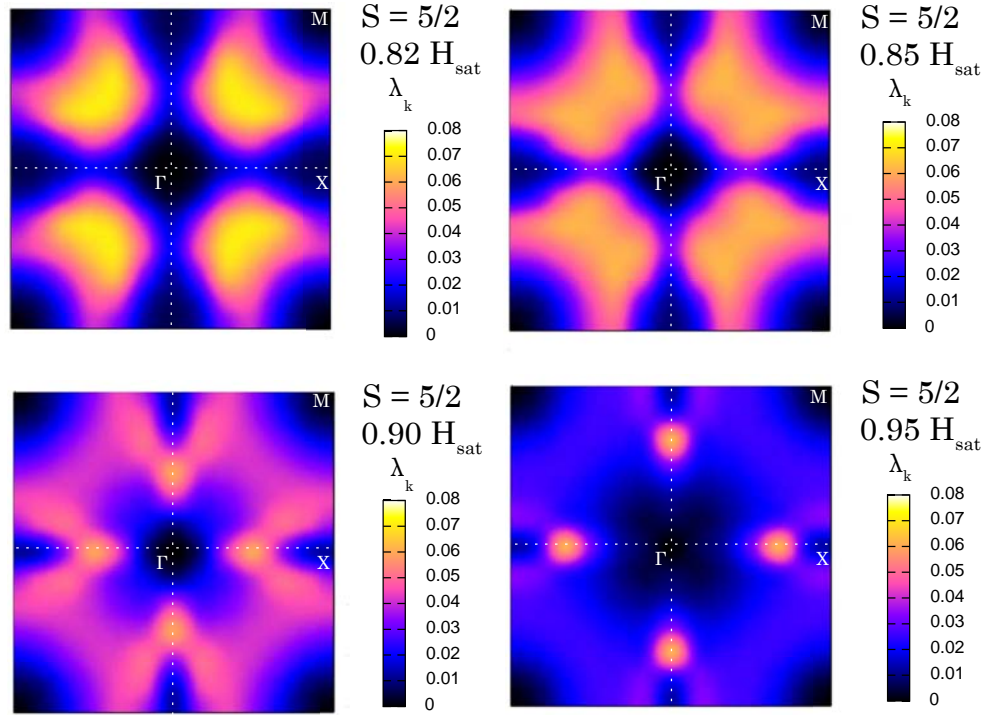


Figure 4.3: Intensity plot in the Brillouin zone of magnons decay rates within the SCBA for spin 5/2. Values for  $\lambda$  are computed on the same grid as for Figure 4.2.

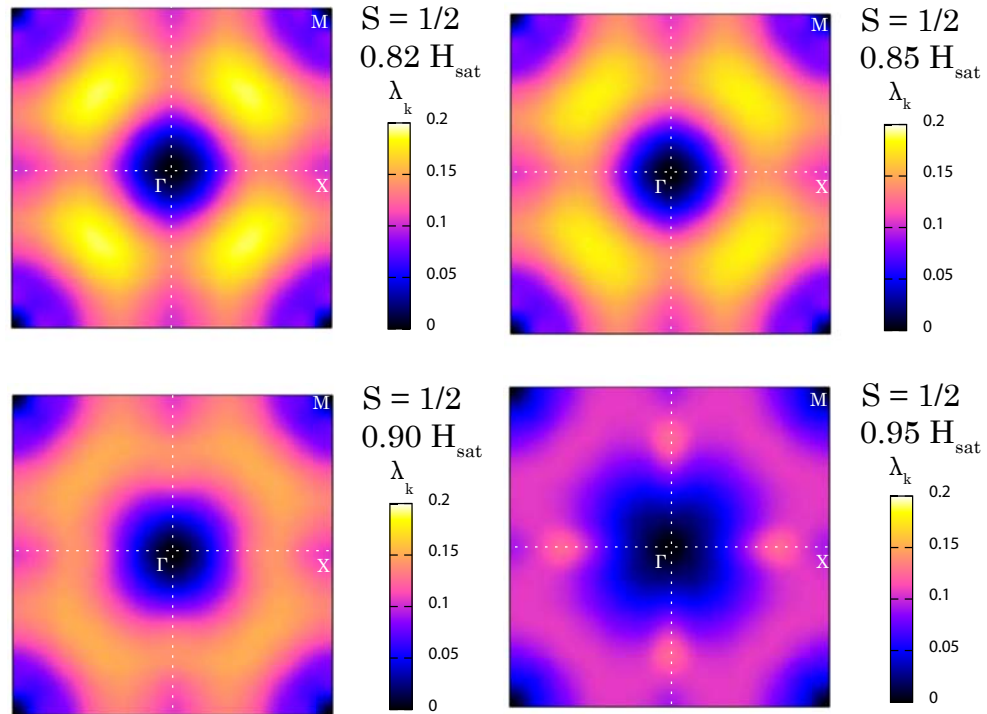


Figure 4.4: Intensity plot in the Brillouin zone of magnons decay rates within the SCBA for spin 1/2. Values for  $\lambda$  are computed on the same grid as for Figure 4.2.



# Chapter 5

## Neutron scattering predictions

### 5.1 Dynamical correlations functions

Neutron scattering partial differential cross section is proportional to spin dynamical correlation function [19]:

$$\frac{d^2\sigma}{d\epsilon d\Omega} \propto [S^{x_0x_0}(\mathbf{q}, \epsilon) + S^{y_0y_0}(\mathbf{q}, \epsilon) + S^{z_0z_0}(\mathbf{q}, \epsilon)]$$

where

$$S^{\alpha\beta}(\mathbf{q}, \epsilon) = \frac{1}{2\pi} \int_{-\infty}^{\infty} dt e^{i\epsilon t} \langle S_{\mathbf{q}}^{\alpha}(t) S_{-\mathbf{q}}^{\beta}(0) \rangle$$

with  $S_{\mathbf{q}}^{\alpha}$  the space Fourier transform of the  $\alpha$  component of a spin operator. According to the fluctuation-dissipation theorem [4] the imaginary part of the spin response function is proportional to the corresponding spin correlations functions so that at zero temperature,

$$\text{Im}\chi^{\alpha\beta}(x, x'|\epsilon) = \frac{1}{2} S^{\alpha\beta}(x, x'|\epsilon) \quad (5.1)$$

where the response function is  $\chi^{\alpha\beta}(x, x'|t - t') = i\theta(t - t') \langle [S^{\alpha}(x, t), S^{\beta}(x', t')] \rangle$ . Combining equation (5.1) with the definition of the spin response functions yields:

$$S^{\alpha\beta}(\mathbf{q}|\epsilon) = 2\text{Im} \int_{-\infty}^{\infty} \frac{dt}{2\pi} e^{i\epsilon t} [i\theta(t - t') \langle [S^{\alpha}(x, t), S^{\beta}(x', t')] \rangle] = -\frac{1}{\pi} \text{Im}\mathcal{F}^{\alpha\beta}(q, \omega) \quad (5.2)$$

where  $\mathcal{F}^{\alpha\beta}$  is the advanced *spin* GREEN's function defined as:

$$\mathcal{F}^{\alpha\beta}(q, \omega) = \int_0^{\infty} dt e^{i\omega t} - i \langle T S_{\mathbf{q}}^{\alpha}(t) S_{-\mathbf{q}}^{\beta} \rangle \quad (5.3)$$

As a result, computing dynamical correlations functions can be done through spin GREEN's function using equation (5.2).

### 5.2 Spin Green's function in the canted frame

Due to the canting with magnetic field the correlations function in the laboratory frame  $(x_0, y_0, z_0)$  are related to those in the canted direction  $(x, y, x)$  via :

$$S^{x_0x_0}(\mathbf{q}, \epsilon) = \cos^2(\theta) S^{zz}(\mathbf{q} - \mathbf{Q}, \epsilon) + \sin^2(\theta) S^{xx}(\mathbf{q}, \epsilon) + \cos(\theta) \sin(\theta) [S^{xz}(\mathbf{q}, -\mathbf{q} + \mathbf{Q}|\epsilon) + S^{zx}(\mathbf{q} - \mathbf{Q}, -\mathbf{q}|\epsilon)] \quad (5.4)$$

$$S^{z_0z_0}(\mathbf{q}, \epsilon) = \cos^2(\theta) S^{xx}(\mathbf{q} - \mathbf{Q}, \epsilon) + \sin^2(\theta) S^{zz}(\mathbf{q}, \epsilon) - \cos(\theta) \sin(\theta) [S^{xz}(\mathbf{q} - \mathbf{Q}, -\mathbf{q}|\epsilon) + S^{zx}(\mathbf{q}, -\mathbf{q} + \mathbf{Q}|\epsilon)] \quad (5.5)$$

where  $S^{\alpha\beta}(\mathbf{q}_1, \mathbf{q}_2|\epsilon) = \frac{1}{2\pi} \int_{-\infty}^{\infty} dt e^{i\epsilon t} \langle S_{\mathbf{q}_1}^{\alpha}(t) S_{\mathbf{q}_2}^{\beta}(0) \rangle$ .

Correlations in the  $y_0$  direction remain unchanged by frame transformation so that  $S^{y_0 y_0}(\mathbf{q}, \epsilon) = S^{yy}(\mathbf{q}, \epsilon)$ . It is therefore necessary to compute several GREEN's functions in the canted frame. They rather concerns *transverse* ( $\mathcal{F}^{xx}$  and  $\mathcal{F}^{yy}$ ), *longitudinal* ( $\mathcal{F}^{zz}$ ) or *mode-coupled* ( $\mathcal{F}^{xz}$ ) fluctuations. The latter fluctuations can be neglected as they only contribute at the second order in perturbation theory.

### 5.2.1 Longitudinal fluctuations

Using HOLSTEIN-PRIMAKOFF (HP) formalism it is easy to write the Fourier Transform of a spin operator in the  $z$  direction as:

$$S_{\mathbf{q}}^z = \frac{\delta_{\mathbf{q},0}}{\sqrt{N}} \left( S - \sum_{\mathbf{k}} a_{\mathbf{k}}^{\dagger} a_{\mathbf{k}} \right) - \frac{1 - \delta_{\mathbf{q},0}}{\sqrt{N}} \sum_{\mathbf{k}} a_{\mathbf{k}}^{\dagger} a_{\mathbf{k}+\mathbf{q}}$$

The product of two different  $S^z$  operators can therefore be separated in *elastic* and *inelastic* parts:

$$S_{\mathbf{q}_1}^z S_{\mathbf{q}_2}^z = N \langle S \rangle \underbrace{\delta_{\mathbf{q}_1,0} \delta_{\mathbf{q}_2,0}}_{\text{elastic}} - \frac{1}{N} \underbrace{(1 - \delta_{\mathbf{q}_1,0})(1 - \delta_{\mathbf{q}_2,0})}_{\text{inelastic}} \sum_{\mathbf{k}_1, \mathbf{k}_2} a_{\mathbf{k}_1}^{\dagger} a_{\mathbf{k}_1+\mathbf{q}_1} a_{\mathbf{k}_2}^{\dagger} a_{\mathbf{k}_2+\mathbf{q}_2}$$

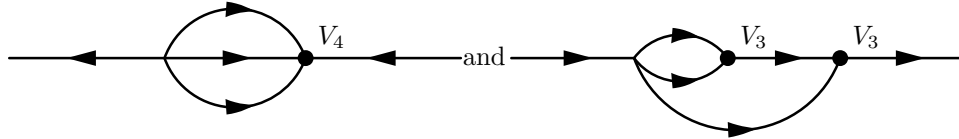
where  $\langle S \rangle$  corresponds to the on-site magnetization with quantum corrections at the  $1/S^0$  order included. Inelastic contributions to the longitudinal spin GREEN's function reads:

$$\mathcal{F}^{zz}(\mathbf{q}_1, \mathbf{q}_2|t) = -\frac{i}{N} \sum_{\mathbf{k}_1, \mathbf{k}_2} \left\langle T a_{\mathbf{k}_1}^{\dagger}(t) a_{\mathbf{k}_1+\mathbf{q}_1}(t) a_{\mathbf{k}_2}^{\dagger} a_{\mathbf{k}_2+\mathbf{q}_2} \right\rangle \quad (5.6)$$

In order to evaluate the ground-state average ( $\langle \dots \rangle$ ) it is necessary to introduce  $b$ -operators in (5.6) with a canonical BOGOLIUBOV transformation. This operation mixes creation and annihilation terms so that the resulting expression contains all possible four  $b$  operators products. In a perturbative expansion the first non-zero terms on the ground state have the following form:

$$\mathcal{F}^{zz} \propto -i \langle b_1 b_2 b_3^{\dagger} b_4^{\dagger} \rangle - \int dt_1 \langle b_1^{\dagger} b_2^{\dagger} b_3^{\dagger} b_4^{\dagger} V_4(t_1) \rangle + \frac{i}{2} \int dt_1 dt_2 \langle b_1 b_2^{\dagger} b_3^{\dagger} b_4^{\dagger} V_3(t_1) V_3(t_2) \rangle + \dots$$

where momentum and time indices are forgotten for simplicity but should be explicitly derived if quantitative results are needed.  $V_4$  and  $V_3^2$  vertices correspond to the following diagrams:



so that  $V_3^3$  and  $V_4$  contributes to the self-energy at orders higher than  $1/S^1$  and can therefore be neglected.

The spin GREEN's function at this order only contains products with two creations and two annihilations operators. Using BOGOLIUBOV's transformation and WICK's theorem to pair  $b$  operators yields:

$$\begin{aligned} \mathcal{F}^{zz}(\mathbf{q}, t) = \frac{i}{N} \sum_{\mathbf{k}} \left\{ [u_{\mathbf{k}} u_{\mathbf{q}+\mathbf{k}} + v_{\mathbf{k}} v_{\mathbf{q}+\mathbf{k}}]^2 \mathcal{G}_{11}(\mathbf{k}, -t) \mathcal{G}_{11}(\mathbf{q} + \mathbf{k}, t) \right. \\ \left. + \frac{1}{2} [u_{\mathbf{q}-\mathbf{k}} v_{\mathbf{k}} + u_{\mathbf{k}} v_{\mathbf{q}-\mathbf{k}}]^2 \mathcal{G}_{11}(\mathbf{k}, t) \mathcal{G}_{11}(\mathbf{q} - \mathbf{k}, t) \right. \\ \left. + \frac{1}{2} [u_{\mathbf{q}+\mathbf{k}} v_{\mathbf{k}} + u_{\mathbf{k}} v_{\mathbf{q}+\mathbf{k}}]^2 \mathcal{G}_{11}(\mathbf{k}, -t) \mathcal{G}_{11}(-\mathbf{q} - \mathbf{k}, -t) \right\} \quad (5.7) \end{aligned}$$

where  $\mathcal{G}_{11}(\mathbf{k}, t) = -i \langle T b_{\mathbf{k}}(t) b_{\mathbf{k}}^\dagger \rangle$  are normal magnons GREEN's function. After time FOURIER transform, equation (5.7) involves three type of GREEN's function products. Since poles of the product  $\mathcal{G}(\mathbf{k}, \epsilon') \mathcal{G}(\mathbf{k} + \mathbf{q}, \epsilon + \epsilon')$  both lies in the lower-half plane, integration with respect to  $\epsilon'$  can be carried out in the upper-half plane as integrated product vanishes so that. The two remaining contributions reads:

$$\begin{aligned} \mathcal{F}^{zz}(\mathbf{q}, \epsilon) = \frac{i}{2N} \sum_{\mathbf{k}} \int_{-\infty}^{\infty} \frac{d\epsilon'}{2\pi} \left\{ \frac{(u_{\mathbf{k}} v_{\mathbf{k}-\mathbf{q}} + u_{\mathbf{k}-\mathbf{q}} v_{\mathbf{k}})^2}{[\epsilon' - \epsilon_{\mathbf{k}} - \Sigma_{11}(\mathbf{k}, \epsilon)] [\epsilon - \epsilon' - \epsilon_{\mathbf{q}-\mathbf{k}} - \Sigma_{11}(\mathbf{k} - \mathbf{q}, \epsilon - \epsilon')]} \right. \\ \left. + \frac{(u_{\mathbf{k}} v_{\mathbf{k}+\mathbf{q}} + u_{\mathbf{k}+\mathbf{q}} v_{\mathbf{k}})^2}{[\epsilon' - \epsilon_{\mathbf{k}} - \Sigma_{11}(\mathbf{k}, \epsilon)] [-\epsilon - \epsilon' - \epsilon_{-\mathbf{q}-\mathbf{k}} - \Sigma_{11}(-\mathbf{k} - \mathbf{q}, -\epsilon - \epsilon')]} \right\} \end{aligned} \quad (5.8)$$

## 5.2.2 Transverse fluctuations

In the HP formalism up to the  $1/S^1$  order, spin operators in the  $x$  and  $y$  directions and in lattice space reads :

$$\begin{aligned} S_i^x &= \frac{1}{2} (S_i^+ + S_i^-) \approx \sqrt{\frac{S}{2}} \left[ a_i^\dagger + a_i - \frac{1}{4S} \left\{ a_i^\dagger a_i^\dagger a_i + a_i^\dagger a_i a_i \right\} \right] \\ S_i^y &= \frac{1}{2i} (S_i^+ - S_i^-) \approx -i \sqrt{\frac{S}{2}} \left[ a_i - a_i^\dagger - \frac{1}{4S} \left\{ a_i^\dagger a_i a_i - a_i^\dagger a_i^\dagger a_i \right\} \right] \end{aligned} \quad (5.9)$$

Using mean-field decoupling with  $n \equiv \langle a_i^\dagger a_i \rangle$  and  $\delta \equiv \langle a_i^\dagger a_i^\dagger \rangle$ , FOURIER transform of spin operators yields :

$$\begin{aligned} S_{\mathbf{q}}^x &= S_{\mathbf{q},1}^x + S_{\mathbf{q},2}^x = \sqrt{\frac{S}{2}} \left[ (a_{-\mathbf{q}}^\dagger + a_{\mathbf{q}}) \left( 1 - \frac{2n + \delta}{4S} \right) \right] \\ &\quad - \frac{1}{4\sqrt{2S}} \frac{1}{N} \sum_{\mathbf{k}_1, \mathbf{k}_2} : \left[ a_{\mathbf{k}_1}^\dagger a_{\mathbf{k}_2}^\dagger a_{\mathbf{k}_1 + \mathbf{k}_2 - \mathbf{q}} + a_{\mathbf{k}_1 + \mathbf{k}_2 - \mathbf{q}}^\dagger a_{\mathbf{k}_2} a_{\mathbf{k}_1} \right] \\ S_{\mathbf{q}}^y &= S_{-\mathbf{q},1}^x + S_{-\mathbf{q},2}^x = -i \sqrt{\frac{S}{2}} \left[ (a_{\mathbf{q}} - a_{-\mathbf{q}}^\dagger) \left( 1 - \frac{2n - \delta}{4S} \right) \right] \\ &\quad + \frac{i}{4\sqrt{2S}} \frac{1}{N} \sum_{\mathbf{k}_1, \mathbf{k}_2} : \left[ a_{\mathbf{k}_1}^\dagger a_{\mathbf{k}_2}^\dagger a_{\mathbf{k}_1 + \mathbf{k}_2 - \mathbf{q}} - a_{\mathbf{k}_1 + \mathbf{k}_2 - \mathbf{q}}^\dagger a_{\mathbf{k}_2} a_{\mathbf{k}_1} \right] : \end{aligned} \quad (5.10)$$

where  $: \dots :$  denotes the fluctuating part of the three operators product *i.e* the restriction to operators with three differents momenta.

In order to be consistent with expressions for the longitudinal part, expansion of  $\mathcal{F}^{xx}$  and  $\mathcal{F}^{yy}$  should be limited to contributions up to the  $1/S^0$  order. As a result  $S_{\mathbf{q},2}^{x(y)} S_{-\mathbf{q},2}^{x(y)}$  products, of order  $1/S^1$ , can be straightforwardly neglected. Remaining terms are of order  $S$  and  $1/S^0$ . After BOGOLIUBOV transformation,  $S_{\mathbf{q},1}^{x(y)} S_{-\mathbf{q},2}^{x(y)}$  terms sum up all different products of magnons creation and annihilation operators of the form  $\langle b_1^{(\dagger)} : b_2^{(\dagger)} b_3^{(\dagger)} b_4^{(\dagger)} : \rangle$ . However, on the contrary to the longitudinal case, restriction to  $\langle b_1 : b_2 b_3 b_4^\dagger : \rangle$  pairings also vanishes on the ground state as at least three momenta are different. It is therefore necessary to go to the first order in  $V_4$  (or second order in  $V_3$ ) to have non-zero contributions on the ground-state. Such terms have

smallness beyond  $\mathcal{O}(1/S^1)$  and can be neglected. The resulting non-zero contributions reads:

$$\begin{aligned}
\langle S_{\mathbf{q}}^x(t)S_{-\mathbf{q}}^x(0) \rangle &\approx \langle S_{\mathbf{q},1}^x(t)S_{-\mathbf{q},1}^x(0) \rangle + \mathcal{O}(1) \\
&= \frac{S}{2} \left(1 - \frac{2n + \delta}{4S}\right)^2 \left\langle \left[ a_{-\mathbf{q}}^\dagger(t) + a_{\mathbf{q}}(t) \right] \left[ a_{-\mathbf{q}}^\dagger(0) + a_{\mathbf{q}}(0) \right] \right\rangle \\
\langle S_{\mathbf{q}}^y(t)S_{-\mathbf{q}}^y(0) \rangle &\approx \langle S_{\mathbf{q},1}^y(t)S_{-\mathbf{q},1}^y(0) \rangle + \mathcal{O}(1) \\
&= -\frac{S}{2} \left(1 - \frac{2n - \delta}{4S}\right)^2 \left\langle \left[ a_{\mathbf{q}}(t) - a_{-\mathbf{q}}^\dagger(t) \right] \left[ a_{\mathbf{q}}(0) - a_{-\mathbf{q}}^\dagger(0) \right] \right\rangle
\end{aligned} \tag{5.11}$$

Performing BOGOLIUBOV and FOURIER transformation, one can easily obtain the following spin GREEN's function :

$$\mathcal{F}^{xx}(\mathbf{q}, \epsilon) = \frac{S}{2} \left(1 - \frac{2n + \delta}{4S}\right)^2 (u_{\mathbf{q}} + v_{\mathbf{q}})^2 [\mathcal{G}_{11}(\mathbf{q}, \epsilon) + \mathcal{G}_{11}(-\mathbf{q}, -\epsilon) + \mathcal{G}_{12}(\mathbf{q}, \epsilon) + \mathcal{G}_{21}(\mathbf{q}, \epsilon)] \tag{5.12}$$

$$\mathcal{F}^{yy}(\mathbf{q}, \epsilon) = \frac{S}{2} \left(1 - \frac{2n - \delta}{4S}\right)^2 (u_{\mathbf{q}} - v_{\mathbf{q}})^2 [\mathcal{G}_{11}(\mathbf{q}, \epsilon) + \mathcal{G}_{11}(-\mathbf{q}, -\epsilon) - \mathcal{G}_{12}(\mathbf{q}, \epsilon) - \mathcal{G}_{21}(\mathbf{q}, \epsilon)] \tag{5.13}$$

where  $\mathcal{G}_{12}(\mathbf{q}, t) = -i \langle T b_{\mathbf{q}}(t) b_{\mathbf{q}} \rangle$  and  $\mathcal{G}_{21}(\mathbf{q}, t) = -i \langle T b_{\mathbf{q}}^\dagger(t) b_{\mathbf{q}}^\dagger \rangle$  are anomalous GREEN's function.

DYSON equation slightly change in precense of *anomalous* GREEN's function. This problem is already know in other bosonic systems where the BOSE condensate provides a source and sink for particles out of the condensate []. The three different GREEN's function involved:

$$\mathcal{G}_{11}(\mathbf{q}, t) = \begin{array}{c} \text{---} \\ \text{---} \\ \text{---} \end{array} \xrightarrow{q} \begin{array}{c} \text{---} \\ \text{---} \\ \text{---} \end{array} \quad \mathcal{G}_{12}(\mathbf{q}, t) = \begin{array}{c} \text{---} \\ \text{---} \\ \text{---} \end{array} \xleftarrow{-q} \begin{array}{c} \text{---} \\ \text{---} \\ \text{---} \end{array} \xrightarrow{q} \begin{array}{c} \text{---} \\ \text{---} \\ \text{---} \end{array} \quad \mathcal{G}_{21}(\mathbf{q}, t) = \begin{array}{c} \text{---} \\ \text{---} \\ \text{---} \end{array} \xrightarrow{q} \begin{array}{c} \text{---} \\ \text{---} \\ \text{---} \end{array} \xleftarrow{-q} \begin{array}{c} \text{---} \\ \text{---} \\ \text{---} \end{array}$$

are linked together by the so-called BELIAEV's equations:

$$\begin{aligned}
\begin{array}{c} \text{---} \\ \text{---} \\ \text{---} \end{array} \xrightarrow{q} \begin{array}{c} \text{---} \\ \text{---} \\ \text{---} \end{array} &= \begin{array}{c} \text{---} \\ \text{---} \\ \text{---} \end{array} \xrightarrow{q} \begin{array}{c} \text{---} \\ \text{---} \\ \text{---} \end{array} + \begin{array}{c} \text{---} \\ \text{---} \\ \text{---} \end{array} \xrightarrow{q} \text{---} \text{---} \text{---} \text{---} \text{---} \xrightarrow{q} \begin{array}{c} \text{---} \\ \text{---} \\ \text{---} \end{array} + \begin{array}{c} \text{---} \\ \text{---} \\ \text{---} \end{array} \xrightarrow{q} \text{---} \text{---} \text{---} \text{---} \text{---} \xleftarrow{-q} \begin{array}{c} \text{---} \\ \text{---} \\ \text{---} \end{array} \xrightarrow{q} \begin{array}{c} \text{---} \\ \text{---} \\ \text{---} \end{array} \\
\begin{array}{c} \text{---} \\ \text{---} \\ \text{---} \end{array} \xleftarrow{-q} \begin{array}{c} \text{---} \\ \text{---} \\ \text{---} \end{array} \xrightarrow{q} \begin{array}{c} \text{---} \\ \text{---} \\ \text{---} \end{array} &= \begin{array}{c} \text{---} \\ \text{---} \\ \text{---} \end{array} \xleftarrow{-q} \text{---} \text{---} \text{---} \text{---} \text{---} \xleftarrow{-q} \begin{array}{c} \text{---} \\ \text{---} \\ \text{---} \end{array} \xrightarrow{q} \begin{array}{c} \text{---} \\ \text{---} \\ \text{---} \end{array} + \begin{array}{c} \text{---} \\ \text{---} \\ \text{---} \end{array} \xleftarrow{-q} \text{---} \text{---} \text{---} \text{---} \text{---} \xleftarrow{-q} \begin{array}{c} \text{---} \\ \text{---} \\ \text{---} \end{array} \xrightarrow{q} \begin{array}{c} \text{---} \\ \text{---} \\ \text{---} \end{array} \\
\begin{array}{c} \text{---} \\ \text{---} \\ \text{---} \end{array} \xrightarrow{q} \begin{array}{c} \text{---} \\ \text{---} \\ \text{---} \end{array} \xleftarrow{-q} \begin{array}{c} \text{---} \\ \text{---} \\ \text{---} \end{array} &= \begin{array}{c} \text{---} \\ \text{---} \\ \text{---} \end{array} \xrightarrow{q} \text{---} \text{---} \text{---} \text{---} \text{---} \xrightarrow{q} \begin{array}{c} \text{---} \\ \text{---} \\ \text{---} \end{array} \xleftarrow{-q} \begin{array}{c} \text{---} \\ \text{---} \\ \text{---} \end{array} + \begin{array}{c} \text{---} \\ \text{---} \\ \text{---} \end{array} \xrightarrow{q} \text{---} \text{---} \text{---} \text{---} \text{---} \xrightarrow{q} \begin{array}{c} \text{---} \\ \text{---} \\ \text{---} \end{array} \xleftarrow{-q} \begin{array}{c} \text{---} \\ \text{---} \\ \text{---} \end{array}
\end{aligned}$$

In the lowest order, singular self-energies involve one-loops diagrams with rather decay ( $\Gamma_1$ ) or source ( $\Gamma_2$ ) vertices (equation 5.14). As the vertices are *real* then  $\Gamma_1 \Gamma_2^* = \Gamma_2 \Gamma_1^*$  resulting in  $\Sigma_{12} = \Sigma_{21}$  and therefore  $\mathcal{G}_{12} = \mathcal{G}_{21}$ .

$$\Sigma_{12}^{(1)} : \begin{array}{c} \Gamma_1 \\ \text{---} \bullet \text{---} \end{array} \begin{array}{c} \text{---} \bullet \text{---} \\ \Gamma_2^* \end{array} \quad \Sigma_{21}^{(1)} : \begin{array}{c} \Gamma_2 \\ \text{---} \bullet \text{---} \end{array} \begin{array}{c} \text{---} \bullet \text{---} \\ \Gamma_1^* \end{array} \tag{5.14}$$

As a result from BELIAEV's equation the normal and anomalous GREEN's function reads:

$$\mathcal{G}_{11}(\mathbf{q}, \epsilon) = \frac{\epsilon + \epsilon_{\mathbf{q}} + \Sigma_{11}(-\mathbf{q}, -\epsilon)}{[\epsilon - \epsilon_{\mathbf{q}} - \Sigma_{11}(\mathbf{q}, \epsilon)] [\epsilon + \epsilon_{\mathbf{q}} + \Sigma_{11}(-\mathbf{q}, -\epsilon)] + \Sigma_{12}^2(\mathbf{q}, \epsilon)} \tag{5.15}$$

$$\mathcal{G}_{12}(\mathbf{q}, \epsilon) = \frac{-\Sigma_{12}(\mathbf{q}, \epsilon)}{[\epsilon - \epsilon_{\mathbf{q}} - \Sigma_{11}(\mathbf{q}, \epsilon)] [\epsilon + \epsilon_{\mathbf{q}} + \Sigma_{11}(-\mathbf{q}, -\epsilon)] + \Sigma_{12}^2(\mathbf{q}, \epsilon)} \tag{5.16}$$

In the expression for longitudinal fluctuations, contribution from product of anomalous GREEN's function have been neglected. It is therefore consistent to neglect  $\Sigma_{12}^2$  and write:

$$\begin{aligned}\mathcal{F}^{xx}(\mathbf{q}, \epsilon) &= \frac{S}{2} \left(1 - \frac{2n + \delta}{4S}\right)^2 (u_{\mathbf{q}} + v_{\mathbf{q}})^2 \left[ \frac{1}{\epsilon - \epsilon_{\mathbf{q}} - \Sigma_{11}(\mathbf{q}, \epsilon)} + \frac{1}{-\epsilon - \epsilon_{-\mathbf{q}} - \Sigma_{11}(-\mathbf{q}, -\epsilon)} \right. \\ &\quad \left. + \frac{2\Sigma_{12}(\mathbf{q}, \epsilon)}{[\epsilon - \epsilon_{\mathbf{q}} - \Sigma_{11}(\mathbf{q}, \epsilon)][\epsilon + \epsilon_{-\mathbf{q}} + \Sigma_{11}(-\mathbf{q}, -\epsilon)]} \right] \\ \mathcal{F}^{yy}(\mathbf{q}, \epsilon) &= \frac{S}{2} \left(1 - \frac{2n - \delta}{4S}\right)^2 (u_{\mathbf{q}} - v_{\mathbf{q}})^2 \left[ \frac{1}{\epsilon - \epsilon_{\mathbf{q}} - \Sigma_{11}(\mathbf{q}, \epsilon)} + \frac{1}{-\epsilon - \epsilon_{-\mathbf{q}} - \Sigma_{11}(-\mathbf{q}, -\epsilon)} \right. \\ &\quad \left. - \frac{2\Sigma_{12}(\mathbf{q}, \epsilon)}{[\epsilon - \epsilon_{\mathbf{q}} - \Sigma_{11}(\mathbf{q}, \epsilon)][\epsilon + \epsilon_{-\mathbf{q}} + \Sigma_{11}(-\mathbf{q}, -\epsilon)]} \right]\end{aligned}\quad (5.17)$$

## 5.3 Measurable Spin Correlations

### 5.3.1 Correlations functions within the SCBA

In the Self-consistent Born approximation presented before, anomalous contribution to self-energies are forgotten and:

$$\Sigma(\mathbf{q}, \epsilon) = \Sigma_{11}^{(1)}(\mathbf{q}, \epsilon) = i\Lambda_{\mathbf{q}} \quad (5.18)$$

For longitudinal GREEN's function (equation 5.8) one can substitute the latter self-energy expression and perform integration on  $\epsilon'$  in the upper-half plane finally to get:

$$\mathcal{F}^{zz}(\mathbf{q}, \epsilon) = \frac{1}{2N} \sum_{\mathbf{k}} \left\{ \frac{(u_{\mathbf{k}}v_{\mathbf{k}-\mathbf{q}} + u_{\mathbf{k}-\mathbf{q}}v_{\mathbf{k}})^2}{[\epsilon - \epsilon_{\mathbf{k}} - \epsilon_{\mathbf{q}-\mathbf{k}} - i(\Lambda_{\mathbf{k}} + \Lambda_{\mathbf{q}-\mathbf{k}})]} + \frac{(u_{\mathbf{k}}v_{\mathbf{k}+\mathbf{q}} + u_{\mathbf{k}+\mathbf{q}}v_{\mathbf{k}})^2}{[\epsilon + \epsilon_{\mathbf{k}} + \epsilon_{-\mathbf{k}-\mathbf{q}} + i(\Lambda_{\mathbf{k}} + \Lambda_{-\mathbf{q}-\mathbf{k}})]} \right\}$$

It follows that the corresponding correlation function can be computed as :

$$S^{zz}(\mathbf{q}, \epsilon) = \frac{1}{2\pi N} \sum_{\mathbf{k}} \left\{ \frac{(u_{\mathbf{k}}v_{\mathbf{k}-\mathbf{q}} + u_{\mathbf{k}-\mathbf{q}}v_{\mathbf{k}})^2 [\Lambda_{\mathbf{k}} + \Lambda_{\mathbf{q}-\mathbf{k}}]}{[\epsilon - \epsilon_{\mathbf{k}} - \epsilon_{\mathbf{q}+\mathbf{k}}]^2 + [\Lambda_{\mathbf{k}} + \Lambda_{\mathbf{q}-\mathbf{k}}]^2} + \frac{(u_{\mathbf{k}}v_{\mathbf{k}+\mathbf{q}} + u_{\mathbf{k}+\mathbf{q}}v_{\mathbf{k}})^2 [\Lambda_{\mathbf{k}} + \Lambda_{\mathbf{q}+\mathbf{k}}]}{[\epsilon + \epsilon_{\mathbf{k}} + \epsilon_{\mathbf{k}+\mathbf{q}}]^2 + [\Lambda_{\mathbf{k}} + \Lambda_{\mathbf{q}+\mathbf{k}}]^2} \right\}$$

For transversal GREEN's function (equation 5.17) the same substitution yields:

$$\begin{aligned}S^{xx}(\mathbf{q}, \epsilon) &= \frac{S}{2\pi} \left(1 - \frac{2n + \delta}{4S}\right)^2 (u_{\mathbf{q}} + v_{\mathbf{q}})^2 \left[ \frac{\Lambda_{\mathbf{q}}}{[\epsilon - \epsilon_{\mathbf{q}}]^2 + \Lambda_{\mathbf{q}}^2} + \frac{\Lambda_{\mathbf{q}}}{[\epsilon + \epsilon_{\mathbf{q}}]^2 + \Lambda_{\mathbf{q}}^2} \right] \\ S^{yy}(\mathbf{q}, \epsilon) &= \frac{S}{2\pi} \left(1 - \frac{2n - \delta}{4S}\right)^2 (u_{\mathbf{q}} - v_{\mathbf{q}})^2 \left[ \frac{\Lambda_{\mathbf{q}}}{[\epsilon - \epsilon_{\mathbf{q}}]^2 + \Lambda_{\mathbf{q}}^2} + \frac{\Lambda_{\mathbf{q}}}{[\epsilon + \epsilon_{\mathbf{q}}]^2 + \Lambda_{\mathbf{q}}^2} \right]\end{aligned}$$

Plots of  $S^{xx}(\mathbf{q}, \epsilon)$  and  $S^{zz}(\mathbf{q} + \mathbf{Q}, \epsilon)$  are presented on Figure (5.1) for spin one-half and  $H = 0.85H_{sat}$ . In the longitudinal part, one can realize how the broadening due to finite lifetimes changes the one-magnon spectrum. Sharp delta peaks at the GOLDSTONE and  $\mathbf{k} = 0$  modes are transformed in lorentzian shaped peaks in the center part of the reciprocal space quarter. In the transverse component, corresponding to the two-magnons continuum, correlation function is reduced by a factor  $\approx 100$ . As a result, going to the laboratory frame, results are expected to be dominated by contribution from the transverse part in the canted frame corresponding to one-magnon spectrum with enhanced linewidth.

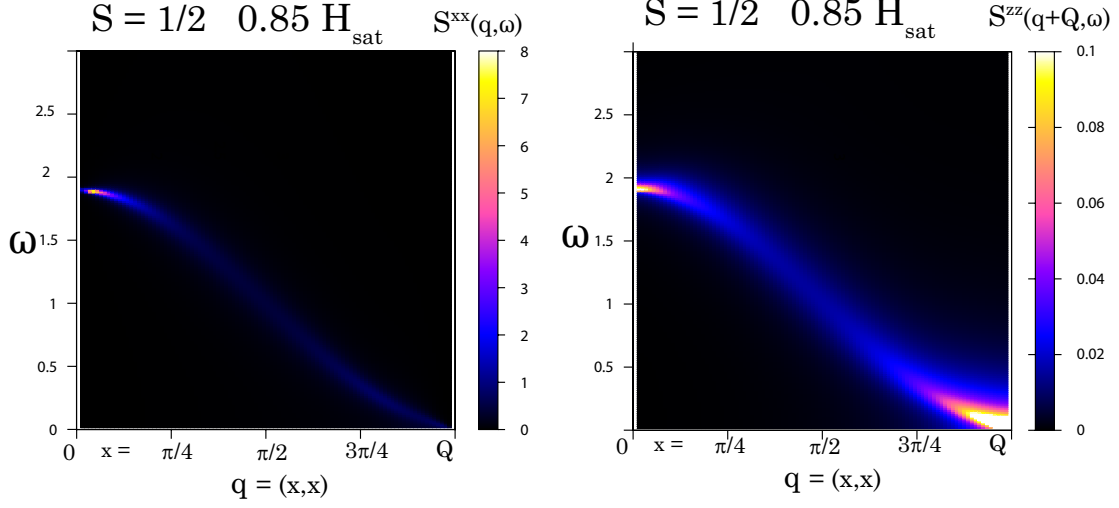


Figure 5.1: Intensity plots of Normalized Dynamical Structure Factor  $S^{xx}(q, \omega)$  and  $S^{zz}(q+Q, \omega)$ . Momenta are chosen on the diagonal of the Brillouin zone. The longitudinal part corresponds to one-magnons excitations whereas the transverse part corresponds to two-magnons continuum. Decay rates used are calculated on a 400x400 grid using the SCBA method

### 5.3.2 Back to the laboratory

With the help of equations (5.4) and (5.5), one can compute the following shape for spin dynamical correlation functions in the laboratory frame (remembering  $S^{yy}$  is unchanged):

$$\begin{aligned}
S^{x_0 x_0}(q, \omega) &= \frac{S \sin^2 \theta}{2\pi} \left(1 - \frac{2n + \delta}{4S}\right)^2 (u_{\mathbf{q}} + v_{\mathbf{q}})^2 \left\{ \frac{\Lambda_{\mathbf{q}}}{[\epsilon - \epsilon_{\mathbf{q}}]^2 + \Lambda_{\mathbf{q}}^2} + \frac{\Lambda_{\mathbf{q}}}{[\epsilon + \epsilon_{\mathbf{q}}]^2 + \Lambda_{\mathbf{q}}^2} \right\} \\
&\quad + \frac{\cos^2 \theta}{2\pi N} \sum_{\mathbf{k}} \left\{ \frac{(u_{\mathbf{k}} v_{\mathbf{k}-\mathbf{q}-\mathbf{Q}} + u_{\mathbf{k}-\mathbf{q}-\mathbf{Q}} v_{\mathbf{k}})^2 [\Lambda_{\mathbf{k}} + \Lambda_{\mathbf{q}-\mathbf{Q}-\mathbf{k}}]}{[\epsilon - \epsilon_{\mathbf{k}} - \epsilon_{\mathbf{q}-\mathbf{Q}+\mathbf{k}}]^2 + [\Lambda_{\mathbf{k}} + \Lambda_{\mathbf{q}-\mathbf{Q}-\mathbf{k}}]^2} \right. \\
&\quad \left. + \frac{(u_{\mathbf{k}} v_{\mathbf{k}+\mathbf{q}-\mathbf{Q}} + u_{\mathbf{k}+\mathbf{q}-\mathbf{Q}} v_{\mathbf{k}})^2 [\Lambda_{\mathbf{k}} + \Lambda_{\mathbf{q}-\mathbf{Q}+\mathbf{k}}]}{[\epsilon + \epsilon_{\mathbf{k}} + \epsilon_{\mathbf{k}+\mathbf{q}-\mathbf{Q}}]^2 + [\Lambda_{\mathbf{k}} + \Lambda_{\mathbf{q}-\mathbf{Q}+\mathbf{k}}]^2} \right\} \\
S^{z_0 z_0}(q, \omega) &= \frac{S \cos^2 \theta}{2\pi} \left(1 - \frac{2n + \delta}{4S}\right)^2 (u_{\mathbf{q}-\mathbf{Q}} + v_{\mathbf{q}-\mathbf{Q}})^2 \left\{ \frac{\Lambda_{\mathbf{q}-\mathbf{Q}}}{[\epsilon - \epsilon_{\mathbf{q}-\mathbf{Q}}]^2 + \Lambda_{\mathbf{q}-\mathbf{Q}}^2} + \frac{\Lambda_{\mathbf{q}-\mathbf{Q}}}{[\epsilon + \epsilon_{\mathbf{q}-\mathbf{Q}}]^2 + \Lambda_{\mathbf{q}-\mathbf{Q}}^2} \right\} \\
&\quad + \frac{\sin^2 \theta}{2\pi N} \sum_{\mathbf{k}} \left\{ \frac{(u_{\mathbf{k}} v_{\mathbf{k}-\mathbf{q}} + u_{\mathbf{k}-\mathbf{q}} v_{\mathbf{k}})^2 [\Lambda_{\mathbf{k}} + \Lambda_{\mathbf{q}-\mathbf{k}}]}{[\epsilon - \epsilon_{\mathbf{k}} - \epsilon_{\mathbf{q}+\mathbf{k}}]^2 + [\Lambda_{\mathbf{k}} + \Lambda_{\mathbf{q}-\mathbf{k}}]^2} \right. \\
&\quad \left. + \frac{(u_{\mathbf{k}} v_{\mathbf{k}+\mathbf{q}} + u_{\mathbf{k}+\mathbf{q}} v_{\mathbf{k}})^2 [\Lambda_{\mathbf{k}} + \Lambda_{\mathbf{q}+\mathbf{k}}]}{[\epsilon + \epsilon_{\mathbf{k}} + \epsilon_{\mathbf{k}+\mathbf{q}}]^2 + [\Lambda_{\mathbf{k}} + \Lambda_{\mathbf{q}+\mathbf{k}}]^2} \right\}
\end{aligned} \tag{5.20}$$

A set of results for transverse mode is presented on Figure (5.2). As in the canted frame, evolution of linewidth for momenta from GOLDSTONE mode to  $\mathbf{k} = 0$  mode is clear. Given the large extension of lorentzian peaks in the middle of  $\Gamma M$  line, neutron scattering techniques can be expected to measure effects of decay.

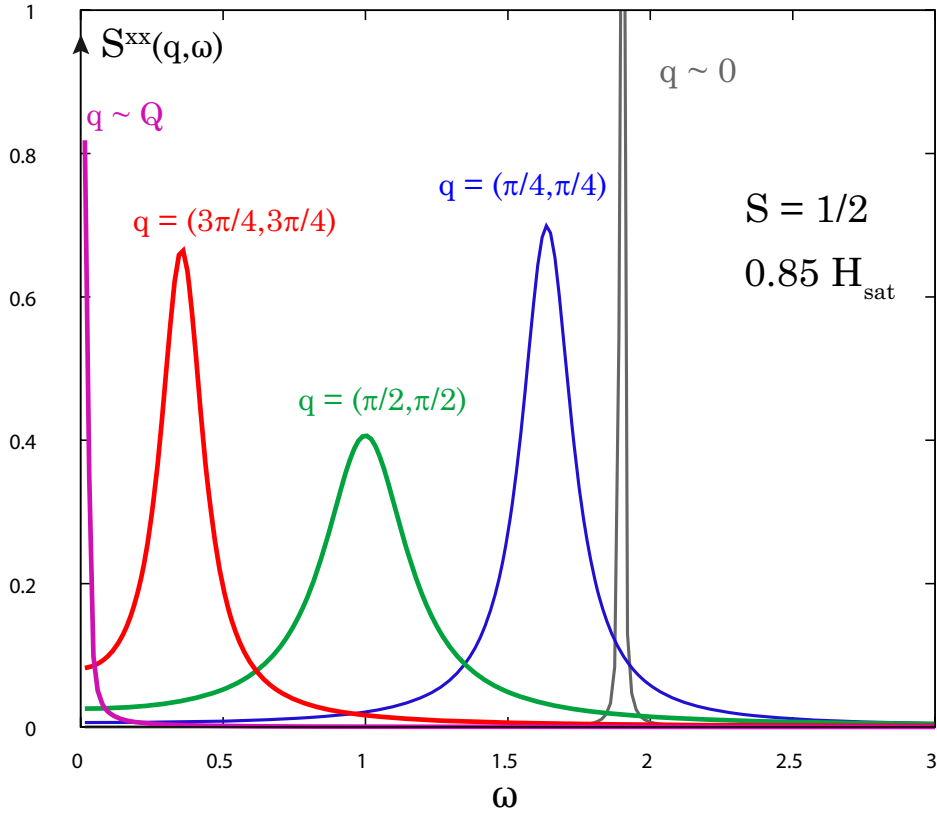


Figure 5.2: Longitudinal part  $xx$  of the dynamical structure factor for spin one-half under  $H = 0.85H_{sat}$ . Energy scan for different momenta on the  $\Gamma M$  line of the BRILLOUIN zone

# Chapter 6

## Conclusion

The present work extended knowledge on the Heisenberg model in studying his behavior under strong magnetic field inducing canted spin structure. Although limited to a bi-dimensional model with nearest-neighbor coupling only, the concepts presented here are believed to be quite general for long-range ordered spin systems with non-collinear structure. Coupling between transverse and longitudinal magnons modes introduce cubic vertices that are the principal interactions of the problem. While combined with quadric terms, these decay and source processes help renormalizing the ground-state energy and the dispersion relation with respect to simple linear spin-wave theory. However, the contribution from decay processes becomes singular above a threshold field  $H^* = 0.76H_{sat}$  where one-magnon excitations become unstable. Instabilities originates from the existence of VAN-HOVE singularities in the two-magnons density of state below the one-magnon energy and one-particle excitations acquire finite lifetime at zero temperature. As concluded from the analysis of kinematic conditions, created magnons are again unstable with respect to spontaneous decay. As a result their decay rate is computed using a Self-Consistent BORN approximation. Near the sound- ( $\mathbf{k} = \mathbf{Q}$ ) and precession- ( $\mathbf{k} = 0$ ) mode one-particle excitations remain well defined whereas strong damping is observed in the middle of the GM line. Resulting dynamical structure factor yields significative broadening of excitation peaks that might be within neutron scattering technique resolution.

Concepts introduced here are quite general and can be extended to tri-dimensional and frustrated systems. More precisely, it is believed that frustration could help lowering the threshold field and therefore provide compounds displaying experimental evidence of such magnons instabilities.



# Bibliography

- [1] M.E. Zhitomirsky A.L. Chernyshev. *Phys. Rev. Letters*, 97(207202), 2006.
- [2] P.W. Anderson. *Phys. Rev.*, 86(5), 1952.
- [3] Birgeneau and al. *Physics Rev. B*, 24(7), 1981.
- [4] P.M Chaikin and T.C.Lubensky. *Principles of Condensed Matter Physics*. Cambridge University Press, 1995.
- [5] A.L. Chernyshev and M.E. Zhitomirsky. *Phys. Rev. Letters*, 82(4536), 1999.
- [6] P. Arndt C.J Hamer, Zheng Weihong. *Phys. Rev. B*, 46(10), 1992.
- [7] L.P. Pitaevskii E.M. Lifshitz. *Statistical Physics Part 2*, volume 9 of *Landau Lifshitz Course of Theoretical Physics*. Pergamon Press, 1980.
- [8] A.A. Abrikosov L.P. Gorkov and I.E Dzyaloshinski. *Methods of Quantum Field Theory in Statistical Physics*. Dover, 1976.
- [9] A. Harrison and al. *Physics Rev. B*, 75(094424), 2007.
- [10] J.I Igarashi and T. Nagao. *Phys. Rev. B*, 72(014403), 2005.
- [11] E.I. Kats and A.R. Muratov. *J.Phys: Condens. Matter*, 17(6849), 2005.
- [12] R. Kubo. *Phys. Rev.*, 87(4), 1952.
- [13] E. Manousakis. *Rev. Mod. Physics*, 63(1), 1991.
- [14] N.D. Mermin and H. Wagner. *Phys. Rev. Letters*, 17(1133), 1966.
- [15] E. Jordao Neves and J. Fernando Perez. *Physics Letters*, 114A(6), 1986.
- [16] N.D. Mermin N.W. Ashcroft. *Solid State Physics*. Brooks Cole, 1976.
- [17] R. Oguchi. *Phys. Rev.*, 117(1), 1960.
- [18] T. Ohyama and H. Shiba. *Journal of the physical society of Japan*, 62(3277), 1993.
- [19] G.L. Squires. *Introduction to the Theory of Thermal Neutron Scattering*. Dover, 1996.
- [20] M.E. Zhitomirsky and T. Nikuni. *Phys. Rev. B*, 57(9), 1998.